

## Nonlinear Dynamics in Atom Optics\*

*Wenyu Chen, S. Dyrting and G. J. Milburn*

Department of Physics, University of Queensland,  
St Lucia, Qld 4072, Australia.

### *Abstract*

In this paper theoretical work on classical and quantum nonlinear dynamics of cold atoms is reported. The basic concepts in nonlinear dynamics are reviewed and then applied to the motion of atoms in time-dependent standing waves and to the atomic bouncer. We describe the quantum dynamics for the cases of regular and chaotic classical dynamics. The effect of spontaneous emission and external noise is also discussed.

### **1. Introduction**

Recent advances in trapping and cooling of neutral atoms have made it possible to observe the spatial variation of the optical dipole force on slow atoms. The effective potentials in which the atoms move are highly nonlinear and vary over the scale of an optical wavelength. Furthermore, the atoms are so cold that they can have a de Broglie wavelength comparable to this scale, and thus the motion can be dominated by quantum effects and cannot be described within the standard semiclassical framework in which Ehrenfest's theorem holds. We can thus expect significant quantum modifications to the classical motion of an atom in an optical dipole potential.

Quantum nonlinear dynamics, however, is very sensitive to environment-induced decoherence. It will only be possible to observe interesting quantum features in nonlinear optical potentials if the atoms are truly isolated from the environment over the timescales of interest. Previous proposals to look for quantum modifications of classical nonlinear dynamics, for example in nonlinear quantum optics, have been difficult to implement as the nonlinearities are so small, and dissipation so large, that quantum coherence effects are destroyed long before any departure from classical behaviour might be expected. In atom optics we are in the opposite situation. Provided the light is sufficiently far from resonance, the atomic motion is very nearly conservative with only a very small irreversible component due to residual spontaneous emission or fluctuations on the light field itself. We are thus faced with the fortunate confluence of large nonlinearities

\* Refereed paper based on a series of lectures presented to the Atom Optics Workshop, held at the Institute for Theoretical Physics, University of Adelaide, in September 1995.

and small dissipation. One final factor makes atom optics an ideal context for quantum nonlinear dynamics: optical potentials may be spatially and temporally modulated with simple optical elements, affording an extraordinary degree of control over the mechanical potentials. Indeed it is possible to deliberately add noise in a controlled manner to determine in detail how the semiclassical limit is established for open quantum systems.

## 2. Hamiltonian Chaos

In this paper we will be investigating the quantum and classical dynamics of a class of nonlinear Hamiltonian systems. The discussion will be restricted to systems with one degree of freedom. Such systems cannot exhibit chaos unless the Hamiltonians are time-dependent. Thus we will consider systems with a potential function which has a higher than quadratic dependence on the position and furthermore we will allow the potential function to be a periodic function of time. This is the simplest class of Hamiltonian system that can exhibit chaotic dynamics.

In practice it is relatively easy to get time-independent potentials in this class. A pendulum moving in a vertical plane under the action of gravity is the classic example. However, achieving periodic temporal modulation of the potential is not so easy. In atom optics, however, the potentials reflect the intensity-dependent induced dipole force on an atom in a light field. The modulation of the resulting mechanical potentials is easily achieved by standard optical modulation techniques. Furthermore, the potentials themselves are almost always non-quadratic in the particle position, as the spatial variation of the light is typically a periodic, and often simply a sinusoidal, function of the position. Thus, while the class of nonlinear systems we will discuss is very special, it also happens to be the appropriate class to describe a wide range of interesting experiments in atom optics.

We first need to define in what sense the systems we will consider are nonlinear. We will only be concerned with nonlinear oscillatory systems, that is, systems for which the position and momentum variables are periodic, but not harmonic, functions of time. Such an oscillator is called nonlinear if the frequency is a function of the energy. This implies that the period of the motion depends on the initial conditions. Periodically driven nonlinear oscillators generically exhibit non-integrable dynamics.

The simplest example of such a nonlinear oscillator is a particle bouncing elastically between two fixed walls and moving freely in between. The period of the oscillator  $T$  is determined by the magnitude of the momentum  $|p|$  of the particle between the walls and the distance between the walls  $d$  as  $T = 2md/|p|$ , where  $m$  is the mass of the particle. Equivalently, we can write the frequency in terms of the energy  $H$  as

$$\omega(H) = \frac{d}{\pi} \sqrt{\frac{m}{H}}. \quad (1)$$

The energy  $H$  for a particle between the fixed walls is just the kinetic energy  $p^2/2m$ . In this case the potential is rather singular, being everywhere zero except at the walls where it is infinite. In practice this is only an approximation to a

smooth potential which rises rapidly over a small region (of atomic dimensions) close to the walls.

The position versus time is a sawtooth oscillatory function while the momentum versus time is a square oscillatory function — clearly non-harmonic. Such non-harmonic functions can always be written as superpositions of harmonic functions with frequencies given by integer multiples of the fundamental frequency. This is simply the Fourier series representation of the non-harmonic oscillation.

When nonlinear oscillators are subjected to periodic forcing, resonances can occur. Of course resonance can occur in a periodically driven simple harmonic oscillator as well, but only at one frequency. By their very nature, resonances can occur far more easily in nonlinear oscillators because they do not have a single fixed frequency, but rather exhibit a range of fundamental frequencies as the initial conditions range over energy. In fact because of the non-harmonic nature of the oscillations, higher-order resonances can occur as the frequency of the driving matches one of many possible higher harmonics in the Fourier decomposition of the natural motion.

We will only consider the simple case where the forcing is harmonic at some fixed frequency  $\Omega$ . Rather than describing the resulting dynamics as a flow in the phase space  $(q, p)$ , far more information is gained if we view the dynamics as a map defined in terms of the position and momentum evaluated at integer multiples of the period,  $\tau = 2\pi/\Omega$ , of the forcing term. This defines the Poincaré map,

$$(q_{n+1}, p_{n+1}) = (f(q_n, p_n), g(q_n, p_n)) , \quad (2)$$

where  $q_n = q(n\tau)$ ,  $p_n = p(n\tau)$  and  $f$  and  $g$  are typically highly nonlinear functions. The dynamics in the Poincaré section in effect filters out the trivial response at the driving frequency. When the strength of the forcing term is zero, the Poincaré map reveals closed curves when the underlying nonlinear frequency of the problem is incommensurate with the driving period, and fixed points when the underlying frequency of the motion is commensurate with the driving period. Which situation obtains depends on the initial energy of the undriven problem. We refer to those surfaces of constant energy which give frequencies that are rational multiples of the map period as *rational* surfaces. All the other surfaces are irrational.

When the driving is turned on, what happens depends on whether the unperturbed motion is on a rational or an irrational surface. The famous KAM theorem (Lichtenberg and Lieberman 1992) tells us that for small-amplitude driving, irrational surfaces simply become distorted. However, rational surfaces break up into a mixture of stable oscillation and unstable motion. It is in this latter case that chaotic dynamics arises.

We can get an idea of what happens by returning to the problem of a particle bouncing elastically between two walls. We can think of this as a particularly dull linear billiard problem with the ball moving on a frictionless horizontal surface between two barriers. To add periodic driving to the problem imagine that we periodically apply a linear attractive or repulsive force. We can model this

by supposing that between the walls the particle is moving in the periodically modulated quadratic potential

$$V(q, t) = \frac{\epsilon}{2} q(t)^2 \sin(\Omega t), \quad (3)$$

where  $\epsilon$  is a positive constant, such that  $\epsilon d^2 \ll 1$ . The billiard table is no longer flat but has a small oscillating 'bump' at the centre.

Between the walls, the total Hamiltonian for the system is

$$H(t) = \frac{p^2}{2m} + \frac{\epsilon q(t)^2}{2} \sin(\Omega t). \quad (4)$$

We will now assume the walls are located at  $q = \pm d/2$ . Hamilton's equations, for motion between the walls, are

$$\begin{aligned} \dot{q} &= \frac{\partial H}{\partial p} = p, \\ \dot{p} &= -\frac{\partial H}{\partial q} = -\epsilon q(t) \sin(\Omega t). \end{aligned}$$

As  $\epsilon$  is small we will try to find a solution which is a perturbation on the solution with no modulation. When  $\epsilon = 0$  the solution for the position  $q^{(0)}(t)$  is a sawtooth function, which can be written as the Fourier series

$$q^{(0)}(t) = \frac{4d}{\pi^2} \sum_{n=0}^{\infty} \frac{(-1)^{2n+1}}{(2n+1)^2} \sin((2n+1)\omega t), \quad (5)$$

where  $\omega$  is the nonlinear frequency.

Suppose now the solution to the perturbed problem can be written as a series in  $\epsilon$ :

$$q(t) = q^{(0)}(t) + \epsilon q^{(1)}(t) + O(\epsilon^2), \quad (6)$$

$$p(t) = p^{(0)}(t) + \epsilon p^{(1)}(t) + O(\epsilon^2). \quad (7)$$

Substituting and equating coefficients of  $\epsilon$  we find

$$\frac{dp^{(1)}(t)}{dt} = -\epsilon q^{(0)}(t) \sin(\Omega t). \quad (8)$$

Using equation (5), this may be written as

$$\frac{dp^{(1)}(t)}{dt} = -\frac{2\epsilon d}{\pi^2} \sum_{n=0}^{\infty} \frac{(-1)^{2n+1}}{(2n+1)^2} (\cos[((2n+1)\omega - \Omega)t] + \cos[((2n+1)\omega + \Omega)t]). \quad (9)$$

A problem is immediately apparent. Each term on the right-hand side of this equation is an oscillatory function of time, *except* those terms for which

$$\Omega = (2n + 1)\omega(H). \tag{10}$$

This term would cause  $p^{(1)}(t)$  to grow linearly in time, leading to a breakdown of the assumption of a small perturbation. The condition in equation (10) is called a resonance and will occur for initial conditions located on a rational surface. Thus the breakup of resonant surfaces under periodic perturbation is associated with a resonance and the failure of perturbation theory in this region of phase space. The new phase-space trajectories are no longer simply a perturbation on those for the undriven problem but reflect a new topological structure entirely. The result is the appearance of new phase-space structures, resonant islands in a sea of chaos. An indication of what can happen is given in Fig. 1 where the square well is approximated by  $\tan^6 q$ . It is through such a topological change in trajectories on resonant surfaces that chaos arises in periodically driven nonlinear oscillators with one degree of freedom.

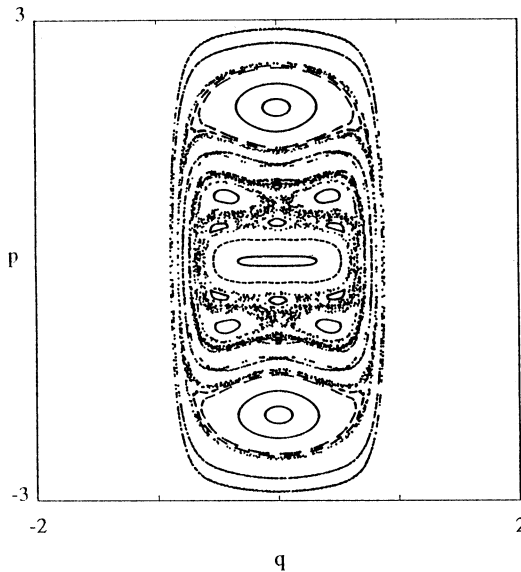


Fig. 1. Poincaré section for a periodically driven nonlinear oscillator, with  $\Omega = 2\pi, \epsilon = 0.8$ .

In determining the dynamics of a nonlinear oscillator we usually make a canonical transformation to new variables,  $(I, \theta)$ , the action–angle variables. The idea is to use variables for which the oscillatory solution is especially simple. In the original phase space,  $(q, p)$ , the trajectories are closed curves. The action variable is chosen so that it is a constant on each closed phase-space trajectory. This is defined to be the area bounded by the trajectory in phase-space divided by  $2\pi$ . The conjugate variable is chosen so that it increases by  $2\pi$  after one orbit of the phase-space curve in  $(q, p)$  space. This ensures that areas are preserved under the transformation to action–angle variables, and thus the transformation is canonical.

In the case of the one-dimensional billiard model discussed above, the phase-space curves are simply rectangles in the  $(q, p)$  phase plane. It is then easy to see that the action variable is given in terms of the energy  $H$  by

$$I(H) = \frac{d\sqrt{2mH}}{\pi}. \quad (11)$$

As  $I$  is only a function of  $H$ , the action must be a constant of motion. The angle variable is defined by  $\theta = \pi|q|/d$ . Hamilton's equations for the new variables are then easily solved to give

$$I(t) = I(0), \quad (12)$$

$$\theta(t) = \theta(0) + \omega(I)t, \quad (13)$$

where

$$\omega(I) = \frac{dH(I)}{dI} \quad (14)$$

is clearly the nonlinear frequency for this initial condition.

The definition of action-angle variables provides an immediate route to quantum mechanics. In Bohr-Sommerfeld quantisation we postulate that the energies of the oscillator are restricted to a discrete set for which the corresponding areas in phase space are (up to an additive constant) integer multiples of Planck's constant. This gives a condition for the allowed action  $I_n$  as

$$I_n = n\hbar + \text{constant}. \quad (15)$$

The constant reflects the ground state, which can be neglected for semiclassical states. In the case of the one-dimensional billiard problem this gives a restriction on the energies,

$$H_n = \frac{\pi^2 n^2 \hbar^2}{2md^2}. \quad (16)$$

It is now easy to see that for semiclassical states the nonlinear frequency of this problem is related to the spacing between energy levels,

$$\omega(H_n) = (H_{n+1} - H_n)/\hbar. \quad (17)$$

This is in fact quite a general result for the semiclassical states of a quantum nonlinear oscillator.

### 3. Nonlinear Dynamics in Atom Optics

In order to avoid the decohering effects of spontaneous emission on the centre-of-mass motion of a cold atom, we will always assume that the optical fields are sufficiently detuned from any atomic resonance. As we will see, this does not completely eliminate the effects of spontaneous emission. The coherent

dynamics for the centre-of-mass and internal states of the atom is generated by the Hamiltonian

$$\hat{H} = \frac{\hat{p}_x^2}{2m} - \frac{\hbar\Delta}{2}\hat{\sigma}_3 - \hbar(\Omega(\hat{x})\hat{\sigma}^\dagger + \Omega(\hat{x})^\dagger\hat{\sigma}) . \quad (18)$$

where  $\Delta$  is the laser–atom detuning and  $\hat{\sigma}_3 = |b\rangle\langle b| - |a\rangle\langle a|$ , with  $a$  labelling the ground state and  $b$  labelling the excited state. The coherent coupling between the internal and centre-of-mass variables is through the position-dependent Rabi frequency  $\Omega(\hat{x}) = \mathbf{d} \cdot \mathbf{E}(\hat{x})/\hbar$ , where  $\mathbf{d}$  is the dipole matrix element for the internal states,  $\mathbf{E}(x)$  is the classical electric field vector at position  $x$  (Kazentsev *et al.* 1990) and the dot is the scalar product of two vectors. We can write the Rabi frequency in the general form

$$\Omega(x) = \Omega f(kx, \tau) , \quad (19)$$

where  $k = c/\omega_L$  is the wavenumber and  $\omega_L$  is the frequency of the laser. Here  $\Omega$  is a measure of the intensity of the field and without loss of generality it can be chosen to be real.

Spontaneous emission is described by the dissipative evolution of the density operator  $\hat{R}$

$$\dot{\hat{R}}_{\text{dis}} = -\gamma\mathcal{L}\hat{R} . \quad (20)$$

The effect of a spontaneous emission is twofold: the atom makes a transition from its internal excited state to its ground state, and the centre-of-mass momentum changes by an amount  $\hbar k\mathbf{n}$ . The direction of the emitted photon  $\mathbf{n}$  is random and has the distribution function (Kazentsev *et al.* 1990)

$$\phi(\mathbf{n}) = \frac{3}{8\pi} \left( 1 - \frac{(\mathbf{d} \cdot \mathbf{n})^2}{\mathbf{d} \cdot \mathbf{d}} \right) . \quad (21)$$

In equation (20)  $\mathcal{L}$  is given by

$$\mathcal{L}\hat{R} = \frac{1}{2} \left( \hat{\sigma}^\dagger\hat{\sigma}\hat{R} + \hat{R}\hat{\sigma}^\dagger\hat{\sigma} - 2\hat{\sigma}\mathcal{N}\hat{R}\hat{\sigma}^\dagger \right) , \quad (22)$$

and  $\mathcal{N}$  is the super operator describing the effect of a spontaneous emission on the transverse momentum of the atom

$$\mathcal{N}\hat{R} = \int \phi(\mathbf{n}) \exp(i\mathbf{n}k\hat{x}) \hat{R} \exp(-i\mathbf{n}k\hat{x}) d\mathbf{n} . \quad (23)$$

For most of the numerical work we chose the ytterbium two-level system suggested in a theoretical paper by Graham *et al.* (1992), for which the fundamental parameters were:  $m = 2.9 \times 10^{-25}$  kg,  $\Omega/2\pi \sim 100$  MHz,  $\Delta/2\pi \sim 1$  GHz,  $\lambda = 556$  nm, and  $\gamma/2\pi = 183$  kHz. In the limit that the detuning  $\Delta$  is much larger than  $\Omega$  the centre-of-mass dynamics is described by an effective Hamiltonian. We further assume that  $\Delta \gg \gamma$ . In this approximation

the evolution of the reduced centre-of-mass density operators  $\hat{\rho}_a = \langle a|\hat{R}|a\rangle$  and  $\hat{\rho}_b = \langle b|\hat{R}|b\rangle$  is given by the coupled equations

$$\begin{aligned} \frac{d\hat{\rho}_a}{dt} = & -\frac{i}{\hbar}[\hat{p}^2/2 + V(\hat{q}, t)/|\nu|^2, \hat{\rho}_a] + \Gamma\mathcal{N}\hat{\rho}_b \\ & -\frac{\eta}{2}[\{f(\hat{q}/2, t)^\dagger f(\hat{q}/2, t), \hat{\rho}_a\} - 2f(\hat{q}/2, t)^\dagger \hat{\rho}_b f(\hat{q}/2, t)], \end{aligned} \quad (24)$$

$$\begin{aligned} \frac{d\hat{\rho}_b}{dt} = & -\frac{i}{\hbar}[\hat{p}^2/2 - V(\hat{q}, t)/|\nu|^2, \hat{\rho}_b] - \Gamma\hat{\rho}_b \\ & -\frac{\eta}{2}[\{f(\hat{q}/2, t)^\dagger f(\hat{q}/2, t), \hat{\rho}_b\} - 2f(\hat{q}/2, t)\hat{\rho}_a f(\hat{q}/2, t)^\dagger], \end{aligned} \quad (25)$$

where  $\nu = 1 - i\gamma/2\Delta$  and  $\{, \}$  denotes the anti-commutator. Following Graham *et al.* (1992) we have introduced the following dimensionless variables for convenience:  $\hbar = (4\hbar k^2/m\omega)$ ,  $\kappa = (\hbar k^2\Omega^2/2m\omega^2\Delta)$ ,  $\Gamma = (\gamma/\omega)$ ,  $t = \omega\tau$ ,  $\eta = (\gamma\Omega^2/4\omega\Delta^2|\nu|^2)$ ,  $q = 2kx$ , and  $p = (2k p_x/m\omega)$ . The operators  $\hat{q}$  and  $\hat{p}$  satisfy the commutation relation

$$[\hat{q}, \hat{p}] = i\hbar. \quad (26)$$

Thus  $\hbar$  plays the role of a dimensionless Planck constant and  $\hat{q}$  and  $\hat{p}$  are the rescaled position and momentum. In the limit of large detuning the reduced density operators  $\hat{\rho}_a$  and  $\hat{\rho}_b$  have been decoupled from the off-diagonal operator  $\langle a|\hat{R}|b\rangle$ . The centre-of-mass observables are fully described by the total density operator  $\hat{\rho} = \hat{\rho}_a + \hat{\rho}_b$ .

When  $\gamma = 0$  we recover the equations for a two-level atom in the large detuning limit coherently interacting with a laser (Kazentsev *et al.* 1980). Without noise due to spontaneous emission the atom is always in the ground state and moves in the potential

$$V(\hat{q}, t) = 2\kappa f(\hat{q}/2, t)^\dagger f(\hat{q}/2, t). \quad (27)$$

When  $\gamma \neq 0$  two more (incoherent) processes are possible: an incoherent stimulated transition between the internal states of the atom at a rate proportional to  $\eta$ , and spontaneous emission from the excited to the ground state, at the rate  $\Gamma$ . In Sections 3 and 4 we review the coherent motion of the atom and set  $\Gamma = 0, \eta = 0$  and  $\nu = 1$ . The effect of spontaneous emission will be treated in Section 5.

### 3.1 Atom in a Standing Wave

The stationary standing wave has a sinusoidal mode function and the optical potential is  $V(\hat{q}, t) = 2\kappa \sin^2(\hat{q}/2)$ . The strength of the potential is proportional to  $\Omega^2$  but inversely proportional to  $\Delta$ , so that when experiments are performed in the limit of large detuning the laser intensity is usually very high.

### 3.1.1 Classical

In the classical approximation to the dynamics we replace the position and momentum operators by  $c$ -number variables  $q$  and  $p$ . Dropping constant terms, the Hamiltonian becomes

$$H = \frac{p^2}{2} - \kappa \cos q . \tag{28}$$

While considerable progress has been made in cooling neutral atoms, we are far from realising a state described by a single point in phase space and we must instead describe classical states by a distribution of points. We therefore define a classical state of the atom to be a probability measure on phase space of the form  $Q(q, p) dq dp$ , where  $Q(q, p)$  is the joint probability density. The density then obeys the Liouville equation (Lichtenberg and Lieberman 1992)

$$\frac{\partial Q}{\partial t} = - \{H, Q\}_{q,p} , \tag{29}$$

where  $\{ , \}_{q,p}$  is the usual Poisson bracket. Let us choose the initial state to be a bivariate gaussian centred on  $(q_0, p_0)$  with position variance  $\sigma_q$  and momentum variance  $\sigma_p$ :

$$Q_0(q, p) = \frac{1}{2\pi\sqrt{\sigma_q\sigma_p}} \exp\left[-\frac{(p-p_0)^2}{2\sigma_p}\right] \exp\left[-\frac{(q-q_0)^2}{2\sigma_q}\right] \tag{30}$$

The solution to (29) is  $Q(q, p, t) = Q_0[\bar{q}(q, p, -t), \bar{p}(q, p, -t)]$ , where  $(\bar{q}(q, p, t), \bar{p}(q, p, t))$  is the trajectory generated by Hamilton's equations. If the initial density is localised in a region of bounded motion it will undergo a rotational shearing. This shearing occurs because points at larger energies (further from the origin in phase space) oscillate with lower frequencies. The resulting pattern is referred to as a 'whorl' (Berry *et al.* 1979). In Fig. 2 we show the effect of nonlinearity on a phase-space distribution for an atom moving classically. The atom is prepared in state (30) with  $(q_0, p_0) = (-1.5, 0)$ ,  $\sigma_q = 0.18$  and  $\sigma_p = 0.33$ . After just ten classical periods it is no longer localised.

An estimate of the shearing rate can be found by assuming that the classical frequency decreases linearly within the region of bounded motion. If the initial localised distribution for the atom has support on an action interval  $\Delta I$  centred on the trajectory  $I$  with classical period  $T_{cl}$ , then it is delocalised when the difference in the angle variable across the distribution is approximately  $2\pi$ . This takes a time  $T_{col}$ , which we call the collapse time, given by

$$T_{col} = T_{cl} \left( \Delta J \left| \frac{d\omega_{cl}}{dE} \right| \right)^{-1} \tag{31}$$

In Fig. 3 we graph the momentum mean and variance as functions of time. We have plotted the statistics at times  $t = 2\pi s$ , with  $s$  integer, and  $s$  is referred to

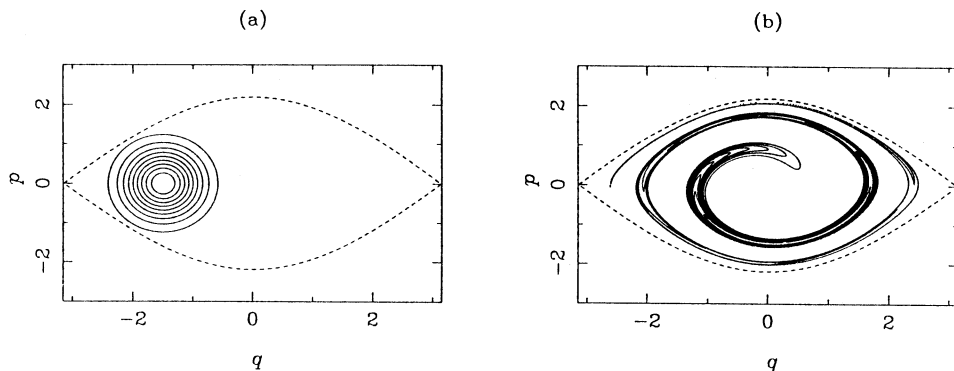


**Fig. 2.** Effect of nonlinear dynamics on the state of the atom represented as a classical distribution in phase space: (a) initially the atom is localised in the region of bounded motion; (b) after just ten classical periods the distribution of the atom is sheared over the trajectories on which it has support.

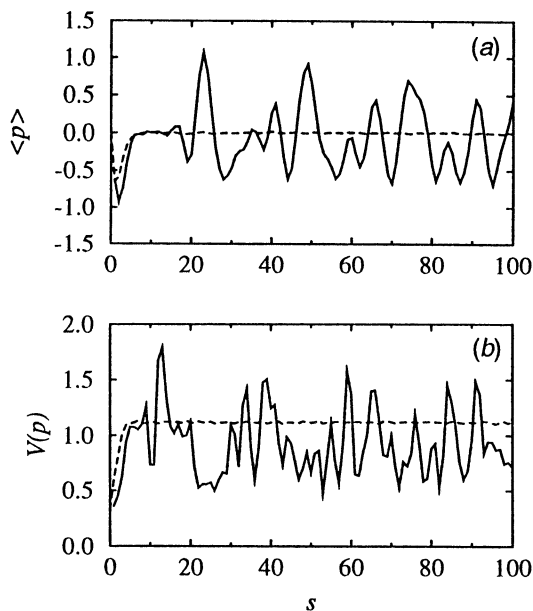


**Fig. 3.** Effect of nonlinear dynamics on the momentum statistics of the atom. A plot of the classical and quantum momentum statistics as a function of strobe number: (a) the mean momentum  $\langle p \rangle$ , and (b) the momentum variance  $V(p)$ . Dashed line, classical mechanics; solid line, quantum mechanics.

as the strobe number. We see that over the collapse time the mean is rapidly damped and the variance rises to a constant value.

### 3.1.2 Quantum

In quantum mechanics we must abandon the possibility of describing the dynamics in terms of phase-space trajectories and must necessarily resort to distributions in phase space. The quantum description is based on the phase-

space dynamics of the  $Q$  function. This is a true phase-space probability density describing simultaneous measurements of position and momentum and is the operational analogue of classical phase-space densities.

The quantum mechanical optical potential is periodic. Hence the translation operator  $\hat{S}_{2\pi} = \exp(-2\pi i \hat{p}/\kappa)$  commutes with the ground-state Hamiltonian

$$\hat{H} = \hat{p}^2/2 - \kappa \cos \hat{q}. \tag{32}$$

It is known (Merzbacher 1970) that the spectrum of a periodic Hamiltonian consists of a countable number of energy bands. Each band is labelled by an integer band number  $n$ . Since the operator  $\hat{S}_{2\pi}$  commutes with the ground-state Hamiltonian, it is possible to choose the eigenstates of  $\hat{H}$  to be eigenstates of  $\hat{S}_{2\pi}$  as well. The translation operator has eigenvalues  $\exp(2\pi i p/\kappa)$  parametrised by the quasi-momentum  $p$ .

The eigenstates  $|E_n, p\rangle$  which diagonalise both  $\hat{H}$  and  $\hat{S}_{2\pi}$  are the Bloch states. Likewise we can use  $n$  and  $p$  to parametrise the energy through the eigenvalue problem

$$\hat{H}|E_n, p\rangle = E_n(p)|E_n, p\rangle. \tag{33}$$

The energy and the Bloch functions repeat themselves in quasi-momentum space. For uniqueness  $p$  is restricted to the first Brillouin zone  $[\kappa/2, -\kappa/2]$  (Kittel 1962). The Bloch states are delocalised in the position representation and this makes it difficult to use them directly to analyse the motion of an atom bound around a single potential minimum. A more useful basis of states are the Wannier states  $|W_n, m\rangle$  found by integrating over the Bloch states in the  $n$ th band (Slater 1952)

$$|W_n, m\rangle = \frac{1}{\sqrt{2\pi\kappa}} \int_{-\kappa/2}^{\kappa/2} \exp(-2\pi i m p/\kappa) |E_n, p\rangle dp. \tag{34}$$

The Wannier state  $|W_n, m\rangle$  is localised at the point  $q = 2\pi m$  and it is easy to verify that it satisfies the translation identity,  $\hat{S}_{2\pi}|W_n, m\rangle = |W_n, m + 1\rangle$ .

We can see how the classical phase space emerges from quantum mechanics by calculating the  $Q$  function of the Wannier states. For a quantum state  $|\psi(t)\rangle$  the  $Q$  function is defined by

$$Q(q, p, t) = \frac{1}{2\pi\kappa} |\langle q, p | \psi(t) \rangle|^2. \tag{35}$$

The states  $|q, p\rangle$  are coherent states (Merzbacher 1970) for a simple harmonic oscillator with frequency chosen as  $\sqrt{\kappa}$ , i.e. the frequency of linear motion around the stable fixed point of the nonlinear pendulum (Walls and Milburn 1994). The  $Q$  function for the Wannier state  $|W_7, 0\rangle$  is plotted in Fig. 4. The phase-space representation of the Wannier state is concentrated about the classical trajectory with the same energy.

Let the energy of the Bloch state  $|E_n, p\rangle$  lie below the height of the optical potential barrier,  $E_n(p) < 2\kappa$ . Using the WKB approximation (Merzbacher 1970)

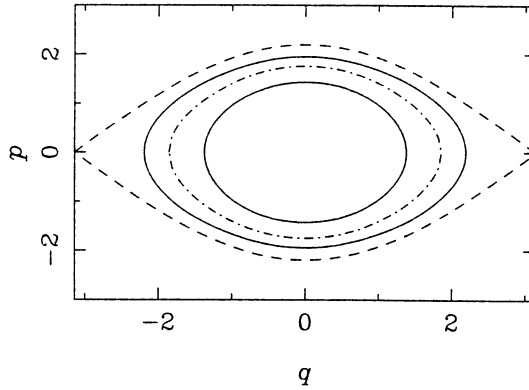


Fig. 4. The  $Q$  function of a bound Wannier state with  $n = 7$ ,  $\bar{E}_n = 1.406$ ,  $\kappa = 1.2$  and  $\hbar = 0.24$ . Solid line,  $Q$  function half-height contour; dashed line, classical separatrix; dot-dashed line, trajectory  $H = \bar{E}_n$ .

the average energy of the  $n$ th band satisfies the Bohr–Sommerfeld quantisation condition

$$I(\bar{E}_n) \approx \hbar(n + \frac{1}{2}). \quad (36)$$

Using (36) the local energy spacing at the  $n$ th band,  $\Delta\bar{E}_n = \bar{E}_n - \bar{E}_{n-1}$ , is related to the classical frequency by

$$\Delta\bar{E}_n \approx \hbar\omega_{\text{cl}}(\bar{E}_n). \quad (37)$$

We will use this expression to define quantum nonlinear motion. If motion of the atom is classically nonlinear then, according to (37), in the semiclassical limit the energy spacing will change with the band number. We illustrate this connection between classical frequency and quantum energy spacings in Fig. 5 where  $\Delta E_n/\hbar$  and  $\omega_{\text{cl}}(\bar{E}_n)$  have been plotted for the nonlinear pendulum. Both the classical and quantum mechanical definitions of nonlinearity are quite general and in the sense of these definitions most physical systems are nonlinear.

We are interested in comparing the classical and quantum dynamics of an atom with a well defined position and momentum. In order to observe genuine quantum nonlinear behaviour we have to wait for a time that is much larger than the classical period. This time has to be long enough that the change in the energy spacing is resolved. The timescale for quantum nonlinear dynamics  $T_{\text{rev}}$  is given by the expression (Littlejohn 1986; Zaslavsky 1985)

$$T_{\text{rev}} = T_{\text{cl}} \left( \frac{\hbar}{2} |\partial\omega_{\text{cl}}/\partial\bar{E}| \right)^{-1}, \quad (38)$$

where  $T_{\text{cl}} = 2\pi/\omega_{\text{cl}}$ . To understand this expression we compare it with the estimation for the collapse time  $T_{\text{col}}$  given by (31). Then  $T_{\text{rev}}$  is the time it takes adjacent energy phasors to become  $4\pi$  out of phase. As our initial state

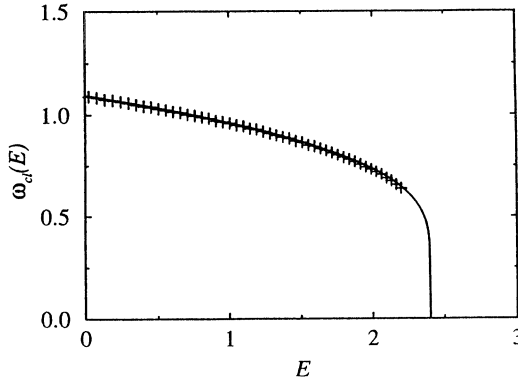


Fig. 5. In a nonlinear quantum mechanical system the energy spacing changes with the principal quantum number,  $\kappa = 1.2$ ,  $\hbar = 0.05$ . The energy difference  $(\bar{E}_n - \bar{E}_{n+1})\hbar$  is plotted as a function of the average band energy  $\bar{E}_n$  and marked by crosses. The energy difference follows the classical frequency.

we choose the minimum uncertainty wave packet

$$\psi(q) = \frac{1}{4\sqrt{2\pi\delta}} \exp \left\{ -(q - q_0)^2/4\delta + ip_0q/\hbar \right\} \tag{39}$$

with means  $q_0$ ,  $p_0$  and position variance  $V(q) = \delta$  and momentum variance  $V(p) = \hbar^2/4V(q)$ . Choose  $p_0 = 0.0$ ,  $q_0 = -1.5$ , and a momentum variance  $\delta = 0.2$ . The  $Q$  function of this state is precisely the classical distribution used in our discussion of classical nonlinear dynamics. In Fig. 2 we have plotted the mean and variance of the momentum as a function of the strobe number for  $\kappa = 1.2$  and  $\hbar = 0.24$ . Note that the quantum mean initially follows the classical mean, but at times  $s \approx 20, 50$  exhibits partial revivals of the initial values. Between these times the momentum variance shows rapid oscillations. Similar behaviour was demonstrated for a Kerr oscillator by Milburn (1985).

Averbukh and Perelman (1989) have shown that when a classical system performs regular periodic motion with a nonlinear frequency, localised wave packets in the semiclassical regime exhibit what they refer to as *fractional revivals* on the characteristic timescale  $T_{\text{rev}}$ . At times  $t = (M/N)T_{\text{rev}}$  with  $M, N$  coprime, the quantum state approximates a superposition of  $L$  copies of the initial state, where

$$L = \begin{cases} N, & N \text{ odd} \\ N/2, & N \text{ even.} \end{cases} \tag{40}$$

This expression is derived by assuming that the atom is bound around the node  $q = 0$ . Since the atom is bound, its state can be written in terms of the Wannier states

$$|\psi(t)\rangle \approx \sum_n a_n \exp(-i\bar{E}_n t/\hbar) |W_n, 0\rangle. \tag{41}$$

One then assumes that the energy varies slowly enough with  $n$  to allow the following semiclassical estimate about the mean quantum number  $\bar{n}$ :

$$\bar{E}_n \approx \bar{E}_{\bar{n}} + \hbar\omega_{\text{cl}}(\bar{E}_{\bar{n}})(n - \bar{n}) + \hbar^2 \frac{\partial \omega_{\text{cl}}}{\partial I}(\bar{E})(n - \bar{n})^2. \quad (42)$$

From equations (31) and (38) we see that the term quadratic in  $n$  is responsible for both the collapse of the momentum mean and for the recombination of the energy phasors at fractional revival times. For an atom in a standing wave the fractional revivals are not perfect, and will degrade with time.

To illustrate fractional revivals in the atomic wavepacket used in Fig. 2, we show in Fig. 6 the contours of the  $Q$  function at times commensurate with the oscillations in the quantum mean and variance. Clearly the state is a superposition of a discrete number of wave packets. For this state  $T_{\text{rev}} = 329$ . This is equivalent to a strobe number  $s \approx 52$  so Fig. 6 corresponds to a fractional revival at time  $t = \frac{1}{4}T_{\text{rev}}$ .

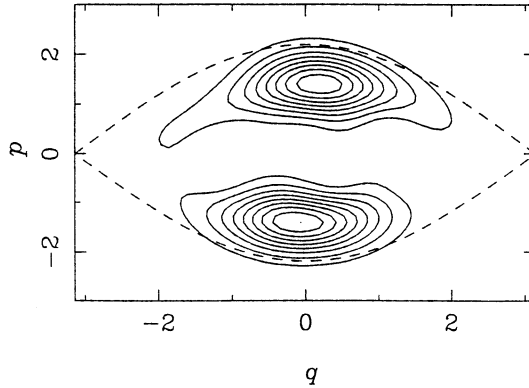


**Fig. 6.** The  $Q$  function for a two-level atom in a stationary standing wave at time  $s = 13$ .

The revivals of the nonlinear pendulum demonstrated above can be realised experimentally by observing the scattering of atoms from an optical standing wave. As an example we propose using ytterbium atoms (Graham *et al.* 1992), a Rabi frequency  $\Omega/2\pi = 1.0 \times 10^8$  Hz, and detuning  $\Delta/2\pi = 2.9 \times 10^9$  Hz. This corresponds to a laser intensity of  $84 \text{ W cm}^{-2}$ . Intensities of this order are already used in atomic cooling experiments (Chen *et al.* 1992). For a characteristic frequency of  $\omega/2\pi = 1.2 \times 10^5$  Hz we have the dimensionless quantities  $\kappa = 1.2$  and  $\hbar = 0.24$ . A wave packet initially localised at  $x = -0.1\lambda$ ,  $\Delta x = 0.02\lambda$ ,  $p_x = 0.0\hbar k$ ,  $\Delta p_x = 3.6\hbar k$  will have a corresponding revival time of  $T_{\text{rev}} = 4.36 \times 10^{-4}$  s. Collimation of the transverse motion of the atom to the degree stated above will be difficult. We require the width of the atomic beam to be  $0.01 \mu\text{m}$  whereas current experiments (Sleater *et al.* 1992) have collimated beams to only  $10 \mu\text{m}$ . To observe the revival at  $t = \frac{1}{4}T_{\text{rev}}$  when the standing wave has dimension 10 mm in the direction of atomic beam propagation the longitudinal velocity of the ytterbium atoms must be  $92 \text{ m s}^{-1}$ .

In Fig. 7 we show the momentum distribution at the fractional revival time of Fig. 6. These peaks would appear as scattering angle data in an experiment.

Our analysis has assumed that dissipation due to spontaneous emission of the atom as it transits the cavity can be neglected.

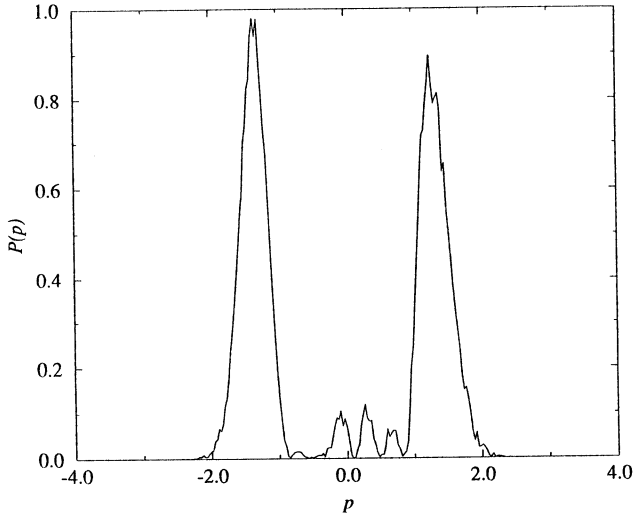


Fig. 7. Scattered momentum distribution for a two-level atom in a stationary standing wave  $t = T_{\text{rev}}/4$ .

### 3.2 Atom Bouncing from an Evanescent Wave

We now discuss an integrable nonlinear system proposed by Wallis *et al.* (1992), which models an atom bouncing vertically from an optical evanescent wave. This is a nonlinear oscillator, as the period of oscillation depends on the initial energy (Chen and Milburn 1995). The nonlinear period is in fact the ‘bounce’ time, which is largely determined by the time taken for the atom to fall onto the evanescent surface from the initial position.

The effective potential felt by the atom has an exponential decay away from the surface. The rate of fall-off of this field is of the order of an optical wavelength over  $2\pi$ . Thus atoms bouncing from a height of the order of millimetres effectively see an infinite boundary at the surface. Of course, if they begin with energy greater than the potential energy at the surface, they hit the dielectric surface supporting the evanescent wave and are not reflected at all. The case of the infinite boundary leads to considerable simplifications in the quantum model, as there exist exact energy eigenstates in terms of Airy functions. We will compare and contrast later the quantum nonlinear dynamics for the infinite potential with the more realistic exponential potential.

In a practical system the reflecting surface is parabolic concave in order to provide stable atomic motion and well defined cavity modes, but in order to simplify the analysis we discuss only the simpler case of flat surface.

#### 3.2.1 The infinite potential case

Infinite potential corresponds to an instantaneous, 100% reflection off a plane

atomic mirror, so the optical potential is

$$V(z) = \begin{cases} mgz & \text{if } z \geq 0 \\ \infty & \text{if } z < 0, \end{cases} \quad (43)$$

where  $m$  is the mass of the atom,  $g$  is the acceleration due to gravity and  $z$  is the distance of the atom from the boundary surface. By setting the potential to infinity at  $z = 0$  we idealise the actual reflecting potential step which may be realised by an evanescent light wave whose extension is typically in the micron range.

Scaling position  $z$  and momentum  $p_z$  by means of the following transformations:  $q = z/\beta$ ,  $p = p_z/m\beta\omega$ , with the position scale  $\beta = \sqrt{\hbar^2/2m^2g}$ , the frequency scale  $\omega = 2\pi mg\beta/\hbar$  and the scaled acceleration  $\mu = g/\beta\omega^2$ , we have the scaled Hamiltonian

$$H = \frac{p^2}{2} + \mu q, \quad q > 0. \quad (44)$$

The Planck parameter is  $\hbar = \hbar/m\beta^2\omega$ . According to Wallis *et al.* (1992), neglecting the internal evolution due to the interaction with the reflecting mirror, the energy eigenstates are in the form of Airy functions, that is

$$\psi_n(q) = \text{Ai}(q - q_n), \quad (45)$$

where  $q_n$  are defined as the solutions to the equation  $\text{Ai}(-q_n) = 0$ .

The energy eigenvalues are  $E_n = mgz_n$ , with  $z_n = \beta q_n$ . The action variable is

$$I(H) = \frac{2H\sqrt{2H}}{3\mu\pi}. \quad (46)$$

By virtue of (14) and (38) the classical period and quantum revival time are

$$T_{\text{cl}} = \frac{2\sqrt{2H}}{\mu}, \quad (47)$$

$$T_{\text{rev}} = \frac{16H^2}{\pi\hbar\mu^2}. \quad (48)$$

### 3.2.2 The exponential potential case

In this case the optical potential for the ground state atom is

$$V(z) = mgz + \varepsilon e^{-\alpha z}, \quad (49)$$

where  $p_z, m, z$  and  $\omega$  are the same as those in Section 3.2.1, and  $\varepsilon$  and  $\alpha$  are the amplitude and decay rate of the evanescent wave respectively. We use the following scaled variables and relations:  $\tilde{q} = \alpha z$ ,  $\tilde{p} = \alpha p_z/m\omega$ , with  $\kappa = \varepsilon\alpha^2/m\omega^2$ ,  $\lambda = \alpha g/\omega^2$  and  $\omega = 2\pi mg/\alpha\hbar$ . Then the effective Hamiltonian in this case is

$$\tilde{H} = \frac{\tilde{p}^2}{2} + \kappa e^{-\tilde{q}} + \lambda\tilde{q}, \quad (50)$$

with the canonical commutation relations  $[\tilde{q}, \tilde{p}] = i\tilde{\hbar}$ , where  $\tilde{\hbar} = \hbar\alpha^2/m\omega$ . In order to ensure that the atoms bounce in the gravitational field if they start from rest, there exists the restriction  $\lambda(1 + \ln(\kappa/\lambda)) < \tilde{H} < \kappa$ .

The scaling scheme here is equivalent to that for the infinite potential case if we choose  $\alpha = 1/\beta$ , which means we have the following correspondence:  $q \sim \tilde{q}, p \sim \tilde{p}, H \sim \tilde{H}, \hbar \sim \tilde{\hbar}$  etc. and for convenience we can use the same variable symbols for the two cases. For the evanescent field analytical formulas are not available so we have to resort to numerical methods.

First we have to find the turning points on the  $q$ -axis  $(q_1, 0)$  and  $(q_2, 0)$  in the classical phase space in order to calculate the action variable, nonlinear frequency etc. Thus we need to solve the equation  $\kappa e^{-q} + \lambda q = H$  around  $(\kappa - H)/(\kappa - \lambda)$  for  $q_1$  and  $H/\lambda$  for  $q_2$ . The action variable is given by

$$I(H) = \frac{1}{\pi} \int_{q_1}^{q_2} \sqrt{2(H - \kappa e^{-q} - \lambda q)} \, dq. \tag{51}$$

The nonlinear frequency is given by (14). The classical period is  $T_{cl} = 2\pi/\omega(H)$ . The quantum revival time is given by (38) with  $\bar{E} = H$ .

### 3.2.3 Fractional revivals

In order to analyse the fractional quantum revivals of the infinite and evanescent potentials we choose the minimum-uncertainty state as the initial state given by (39) with position variance  $V(q) = 1$  and momentum variance  $V(p) = \hbar^2/4$ . We choose the following parameters:  $p_0 = 0, \hbar = 2$  and  $\mu = \lambda = 2$ . In all cases we choose  $\kappa = 100$ . If we make the infinite potential approximation, then the bounce time and the revival time are given by

$$T_{cl} = 2\sqrt{q_0}, \tag{52}$$

$$T_{rev} = \frac{8q_0^2}{\pi}. \tag{53}$$

The above formulas are used in our numerical examples.

The quantum dynamics is easily determined by expanding the initial state in terms of the energy eigenstates. Thus

$$\psi(q, t) = \sum_{n=1}^{\infty} c_n \text{Ai}(q - q_n) e^{-iq_n t}, \tag{54}$$

with  $c_n = \int_{-\infty}^{\infty} \psi(q, 0) \text{Ai}(q - q_n) dq$  and the time scaled in units of  $\hbar/mg\beta$ . The momentum representation  $\psi(p, t)$  of the state at any time is then found by Fourier-transforming  $\psi(q, t)$ . We then calculate the position and momentum probability densities at a quarter of the revival time  $t = \frac{1}{4}T_{rev}$ .

In Figs 8 and 9 we show the position and momentum distribution at one-quarter of the revival time for various initial states. In each case the dashed line

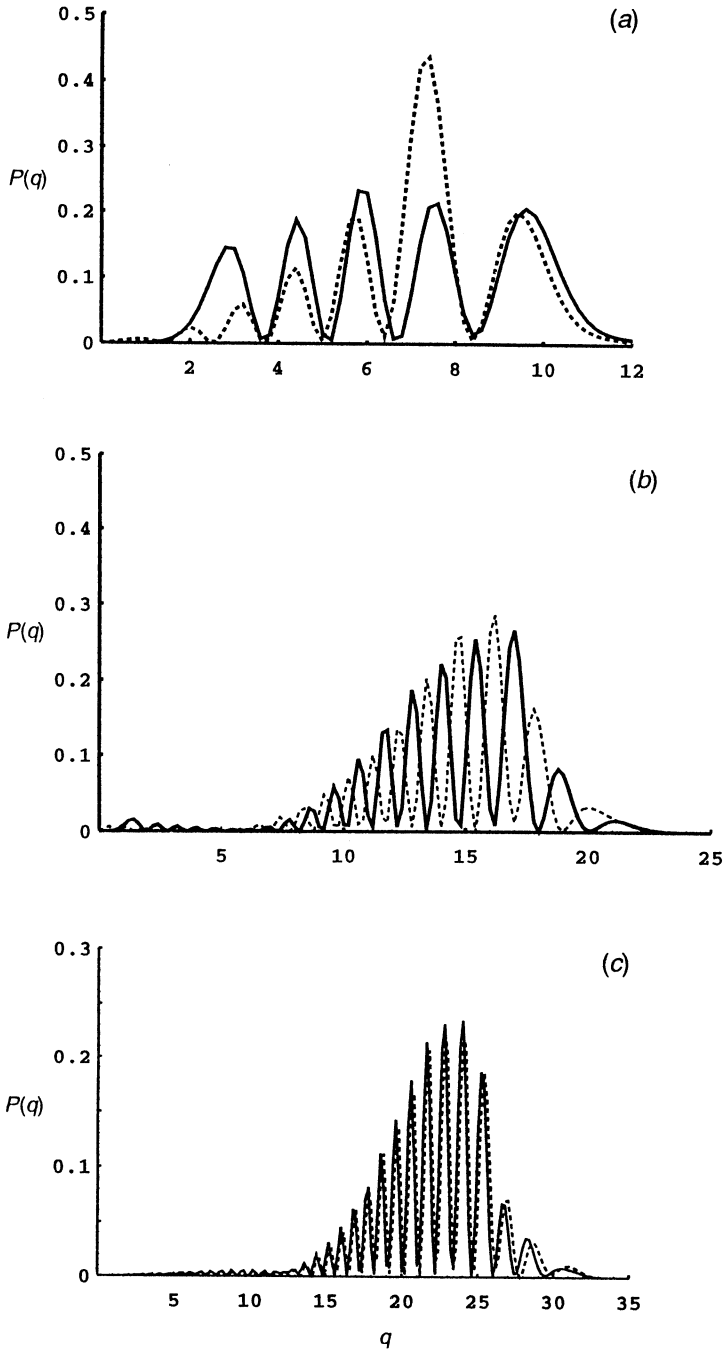


**Fig. 8.** Position probability distributions at one-quarter of the revival time for various initial conditions (a)  $q_0 = 10$ , (b)  $q_0 = 20$  and (c)  $q_0 = 30$ . The dashed line is for the infinite potential and the solid line for the exponential potential.

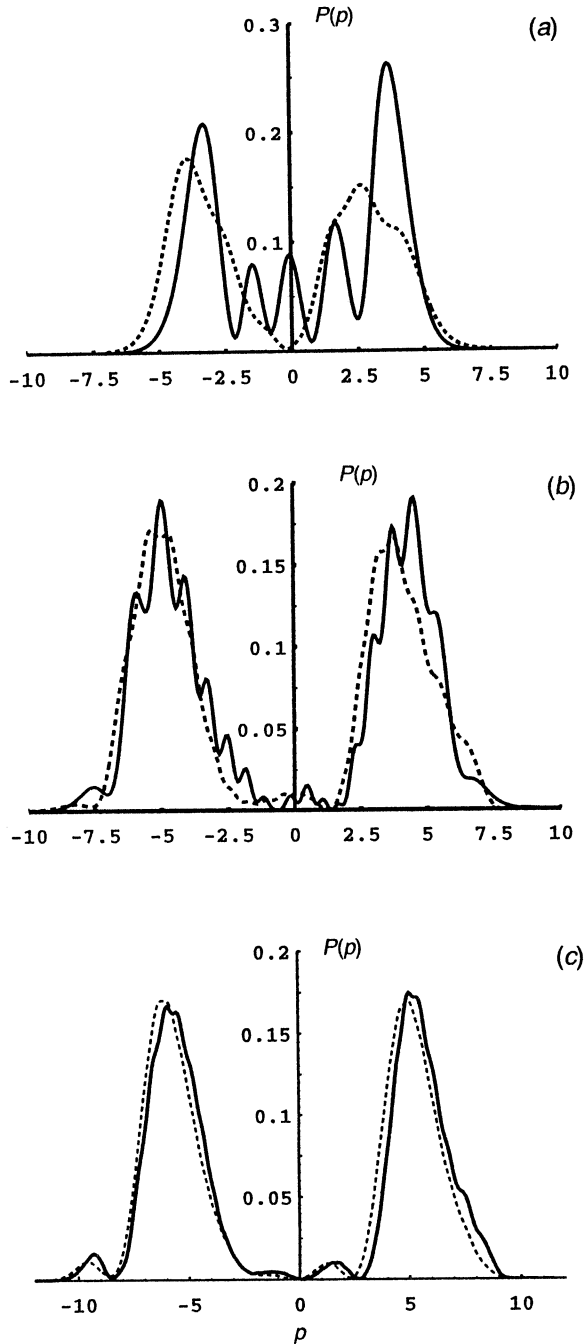


**Fig. 9.** Momentum probability distributions at one-quarter of the revival time for various initial conditions: (a)  $q_0 = 10$ , (b)  $q_0 = 20$  and (c)  $q_0 = 30$ . The dashed line is for the infinite potential and the solid line for the exponential potential.

corresponds to the infinite potential case. Note that the momentum distribution is dominated by two symmetrically placed peaks. This corresponds to the formation of a superposition of two localised states, at the same position, of oppositely directed momentum. In position space this superposition is manifest as a single peak modulated by interference fringes.

For the exponential potential we must calculate the bounce time numerically. In Figs 8 and 9 we show the position and momentum probability distributions at one-quarter of the revival time. In each case the solid line corresponds to the exponential case. As in the infinite case one sees the formation of a superposition of two states of oppositely directed momentum. Comparing Figs 8 and 9, it is clear that as the initial state is located further from the surface, the infinite and exponential cases become increasingly similar. The interference fringes in the position probability distributions for the infinite potential are shifted with respect to those for the exponential case. This is because the classical turning points in the two cases are not the same and because it is not easy to choose the revival time the same in the two cases, due to slight differences in the nonlinear oscillation frequencies of the two models. However, the case  $q_0 = 30$  does show good agreement.

The superposed states are localised and consist of equal but oppositely directed mean momenta. Such a state could possibly be detected by looking for Doppler-shifted resonances with a weak probe, or perhaps the position density fringes could be probed directly.

The practical parameters for our numerical examples are  $z: 0.2 \sim 18 \mu\text{m}$ ,  $T_{\text{cl}}: 0.6 \sim 18 \text{ms}$ ,  $T_{\text{rev}}: 25 \text{ms} \sim 1.6 \text{s}$ ; 10  $\sim$  115 bounces will be needed to see the revivals. The presently available maximum number of bounces is about 10 and seems hopeful but the problem is how to start the atoms extremely close to the surface or even on the surface. One possible solution is to use grazing incidence. Aminoff *et al.* (1993) start the atoms at a height of 3 mm. Then  $q_0 \approx 10^4$ ,  $T_{\text{cl}} \approx 10 \text{ms}$  and  $T_{\text{rev}} \approx 40 \text{s}$ , and in this case the revivals are manifest after  $10^5$  bounces. This is still much beyond experiments presently accessible. In particular, losses such as spontaneous emission would have long since scattered most atoms from the system. There is still a long way to go before practical experiments showing fractional revivals in the atomic bouncer system can be performed.

#### 4. Chaotic Dynamics in Atom Optics

We will discuss three different routes to chaos for an atom moving in an optical potential: (i) by modulating the intensity of the standing wave, (ii) by modulating the nodal positions of the standing wave, and (iii) by modulating the intensity of an evanescent wave. In these cases the potential becomes periodic in time and thus we expect to see a progression to chaos through the break-up of resonant surfaces.

##### 4.1 Standing Wave with Modulated Intensity

If we consider the classical description for the ground-state atom in a standing wave with modulated intensity then the Hamiltonian is

$$H(t) = \frac{p^2}{2} - \kappa(1 - 2\epsilon \cos \Omega t) \cos q. \quad (55)$$

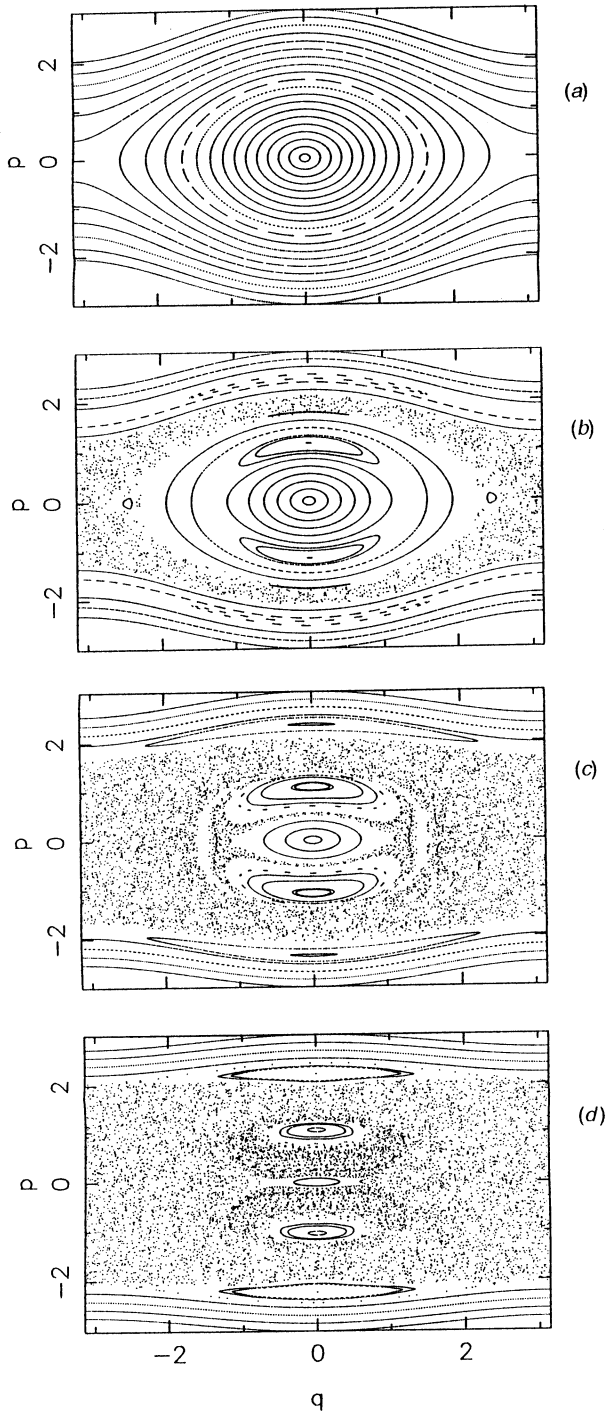


**Fig. 10.** Classical stroboscopic phase portraits for (a)  $\epsilon = 0.0$ , (b)  $\epsilon = 0.1$ , (c)  $\epsilon = 0.2$  and (d)  $\epsilon = 0.3$ .

For non-zero  $\epsilon$  the coupling of the driving term with the motion of the stationary standing wave leads to a change in the topology of rational curves. The overlap of resonances leads to the formation of a layer of stochastic motion about the classical separatrix. The resonances that do not overlap persist as stable regions of phase space.

Henceforth we fix  $\kappa = 1.2$  and study the stroboscopic dynamics as  $\epsilon$  is increased. In Fig. 10 we show the classical stroboscopic phase portraits for  $\epsilon = 0.0, 0.1, 0.2$  and  $0.3$ . Elliptic fixed points are evident about the regions  $(q, p) \approx (0, 0)$ ,  $(q, p) \approx (0, \pm 1.2)$  and  $(q, p) \approx (0, \pm 2.2)$ .

To determine whether first-order resonances occur we Fourier-analyse the first-order (in  $\epsilon$ ) term, i.e.  $\epsilon H_1(I, \theta, t)$ :

$$H_1 = \sum_{m=0, \pm 1, \pm 2, \dots} H_{1,2m}(\exp i(t + 2m\theta) + c.c.). \quad (56)$$

Then first-order resonance solutions occur for  $I$  given by

$$2m\omega_{\text{cl}}(I) - 1 = 0; \quad m = 0, \pm 1, \pm 2, \dots \quad (57)$$

To determine whether second-order resonances occur we must first find approximate action-angle variables  $(\bar{I}, \bar{\theta})$  for  $H(I, \theta, t)$  up to and including the order  $\epsilon$  terms. Provided  $I$  is not close to a first-order resonance, we can do this through a canonical transformation so that the new Hamiltonian is

$$\bar{H}(\bar{I}, \bar{\theta}, t) = H_0(\bar{I}) + \epsilon^2 H_2(\bar{I}, \bar{\theta}, t) + \dots \quad (58)$$

The canonical transformation has introduced an  $\epsilon^2$  term into the new Hamiltonian:  $\epsilon^2 H_2$ . It is the Fourier analysis of this term that shows the second-order resonance solutions. Here

$$H_2 = \sum_{m=0, \pm 1, \pm 2} H_{2,2m}(\exp i(2t + 2m\theta) + c.c.) + \text{time independent terms}, \quad (59)$$

so second-order resonances occur for  $\bar{I}$  given by

$$m\omega_{\text{cl}}(\bar{I}) - 1 = 0; \quad m = 0, \pm 1, \pm 2, \dots \quad (60)$$

For  $\epsilon$  small, first-order resonances are typically more important than second-order resonances. However, for the system we have here, all the first-order resonances are clustered near the separatrix. For  $\epsilon = 0.1$  they have overlapped to form a chaotic band as seen in Fig. 10*b* but there is one second-order resonance  $\omega_{\text{cl}}(\bar{I}) = \pm 1$  at a significantly smaller value of  $\bar{I}$  which is important. The two stable periodic points that replace the invariant appear in Fig 10*b* as fixed points of the stroboscopic map at  $(q, p) \approx (0.0 \pm 1.2)$  and the width of the resonance is surprisingly large,  $\approx 0.44$ .

In Fig. 11 we have plotted the momentum mean  $\langle p \rangle$  and variance  $V(p)$  as a function of the strobe number  $s$  for a cloud of 1000 points evolving under the classical dynamics. The points have an initial density given by (30) with means  $(q_0, p_0) = (0.0, 1.0)$  and variances  $\sigma_q = 0.084$  and  $\sigma_p = 0.036$ .

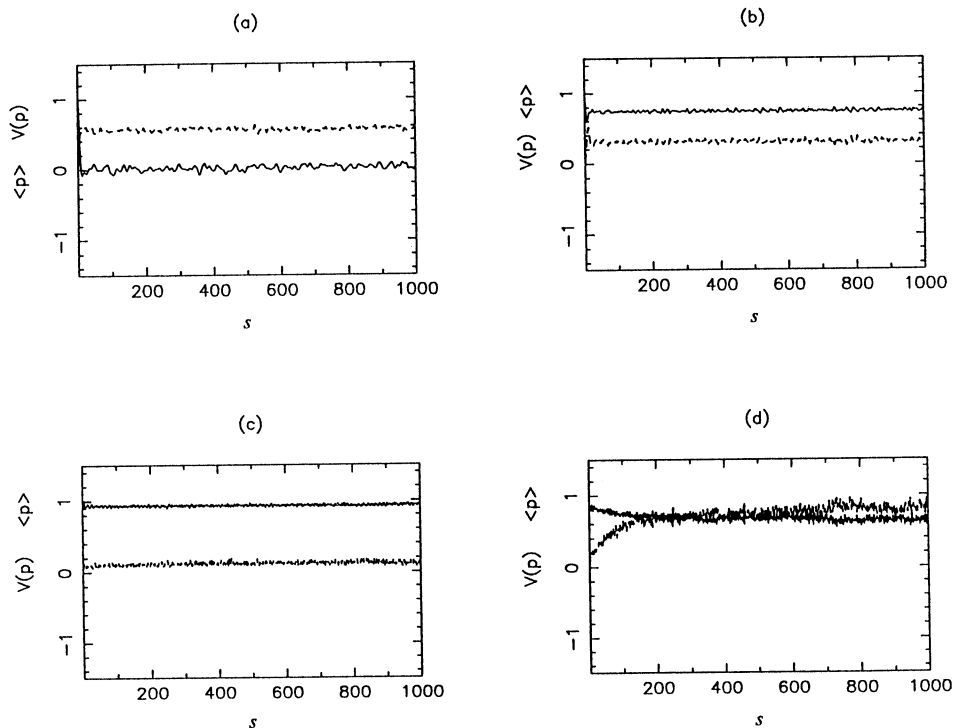


**Fig. 11.** Plot of classical momentum statistics versus strobe number  $s$ : (a)  $\epsilon = 0.0$ , (b)  $\epsilon = 0.1$ , (c)  $\epsilon = 0.2$  and (d)  $\epsilon = 0.3$ . Solid line,  $\langle p \rangle$ ; dashed line,  $V(p)$ .

When  $\epsilon = 0.0$  we see that the mean momentum quickly drops to zero and the momentum variance rises. As the perturbation parameter  $\epsilon$  is increased from 0.0 to 0.2, the width of the stable region is increasing linearly with  $\epsilon$  until the classical distribution is contained within the region of the elliptic fixed point, the growth in momentum variance is suppressed and the mean momentum remains near its initial value. When  $\epsilon$  is increased to 0.3 the stable region of phase space begins to shrink; as a result we see in Fig. 11d that the classical distribution becomes delocalised again.

The quantum analogue of the classical iterative map is the evolution operator

$$\hat{F} = \hat{U}(2\pi), \tag{61}$$

where  $\hat{U}(t)$  is the unitary evolution operator generated by  $\hat{H}(t)$  which evolves quantum states from  $t = 0$  to time  $t$ . The eigenstates of  $\hat{F}$ , denoted by  $|e_n, p\rangle$  for  $n = 0, 1, 2, \dots$ , and quasi-momentum  $p \in [-\hbar/2, \hbar/2]$ , which satisfy

$$\hat{F}|e_n, p\rangle = \exp(-i2\pi e_n(p)) |e_n, p\rangle, \tag{62}$$

provide a convenient basis for studying the stroboscopic evolution. An arbitrary state  $|\psi\rangle$  evolves to

$$\hat{F}^s|\psi\rangle = \sum_{n,p}^{\infty} \exp(-i2\pi s e_n(p)) |e_n, p\rangle \langle e_n, p|\psi\rangle \quad (63)$$

after  $s$  cycles of the driving term.

Notice that when  $\epsilon = 0$  the quantum stroboscopic map  $\hat{F}$  is simply

$$\hat{F} = \exp(-i2\pi \hat{H}_0/\hbar), \quad (64)$$

where  $\hat{H}_0$  is given by (32). Then  $|E_n, p\rangle$  is a quasi-stationary state for  $\hat{F}$  with quasi-energy  $e_n(p) = E_n(p)$ . In analogy with time-independent quantum perturbation theory we assume that for small  $\epsilon$  the perturbed quasi-stationary states  $|e_n, p\rangle$  and quasi-energy  $e_n(p)$  are close to  $|E_n, p\rangle$  and  $E_n(p)$  respectively, and then attempt to find corresponding asymptotic expansions.

Let  $|e_n, p, t\rangle$  denote the state evolving from the initial quasi-stationary state  $|e_n, p\rangle$  under the time-dependent dynamics generated by the Hamiltonian

$$\hat{H}(t) = \hat{H}_0 + \epsilon \hat{H}_1(t), \quad (65)$$

where  $\hat{H}_1(t) = 2\kappa \cos t \cos \hat{q}$ . We introduce states  $|v_n, p\rangle = \exp(i e_n(p)t) |e_n, p\rangle$  which are periodic in  $t$ . These states are solutions of the eigenvalue problem

$$e_n(p) |v_n, p\rangle = \hat{K} |v_n, p\rangle, \quad (66)$$

where  $\hat{K} = \hat{h} + \hat{H}(\hat{t})$ ,  $\hat{h} = -i\hbar d/dt$ . Once the eigenvalue problem (66) has been solved we can recover the quasi-stationary state  $|e_n, p\rangle$  by the projection  $|e_n, p\rangle = |v_n, p\rangle_{t=0}$ .

To solve the eigenvalue problem perturbatively we diagonalise the ‘free’ operator  $\hat{K}_0 = \hat{h} + \hat{H}_0$ . Without loss of generality we look for eigenstates of  $\hat{K}$  that reduce to  $|E_n, p\rangle$  in the limit as  $\epsilon$  vanishes. We assume that  $|v_n, p\rangle$  has the following asymptotic expansions:

$$|v_n, p\rangle = |E_n, p\rangle + \epsilon |v_n^{(1)}, p\rangle + \epsilon^2 |v_n^{(2)}, p\rangle + O(\epsilon^3). \quad (67)$$

The new quasi-stationary states are then calculated using quantum perturbation theory. Up to second order the corrections are (Merzbacher 1970)

$$|e_n^{(1)}, p\rangle = \hat{A}_n^{(1)} |E_n, p\rangle, \quad (68)$$

$$|e_n^{(2)}, p\rangle = \hat{A}_n^{(2)} |E_n, p\rangle, \quad (69)$$

where

$$\hat{A}_n^{(1)} = \sum_l \frac{1}{E_n(p) - \hat{H}_0 - \hbar l} (1 - \delta_{l0} \hat{P}_n(p)) \hat{H}_{1l}, \tag{70}$$

$$\begin{aligned} \hat{A}_n^{(2)} = & - \sum_k \frac{1}{E_n(p) - \hat{H}_0 - \hbar k} (1 - \delta_{k0} \hat{P}_n(p)) \\ & \times \left( e_n^{(1)}(p) \frac{1}{E_n(p) - \hat{H}_0 - \hbar k} (1 - \delta_{k0} \hat{P}_n(p)) \hat{H}_{1k} \right. \\ & \left. - \sum_l \hat{H}_{1l}^\dagger \frac{1}{E_n(p) - \hat{H}_0 - \hbar(k-l)} (1 - \delta_{kl} \hat{P}_n(p)) \hat{H}_{1k-l} \right). \end{aligned} \tag{71}$$

In the above equations  $\hat{P}_n(p) = |E_n, p\rangle\langle E_n, p|$  denotes the projection onto  $|E_n, p\rangle$ ,  $\hat{H}_{1l}$  is the Fourier component of  $\hat{H}_1$  rotating at frequency  $l$ , and  $e_n^{(1)}(p)$  is the first-order correction to the quasi-energy.

The matrix elements  $\langle E_{n'}, p | \hat{A}_n^{(1)} | E_n, p \rangle$  and  $\langle E_{n'}, p | \hat{A}_n^{(2)} | E_n, p \rangle$  become singular when the free energy levels satisfy the resonance condition  $E_n(p) - E_{n'}(p) = \hbar l$ . We will call them first- or second-order resonances depending at which order the singularity occurs. A quantum resonance indicates that the Hamiltonian  $K_0$  has degenerate energy levels. In this case we must use degenerate perturbation theory to find the new quasi-stationary states. When there is a classical second-order resonance (60) for  $m = \pm 1$  we see from (37) that there will be energy levels satisfying

$$\bar{E}_n - \bar{E}_{n\mp 2} \approx \pm 2\hbar. \tag{72}$$

We see from (71) that these states give rise to near-resonant denominators in the second order of quantum perturbation theory ( $k = \pm 2, l = \mp 1$ ). For the quantum dynamics of (55) we take  $\hbar = 0.05$ . We have graphed the quantum mean  $\langle \hat{p} \rangle$  and variance  $V(\hat{p})$  of momentum as a function of the strobe number  $s$  in Fig. 12. When  $\epsilon = 0.0$  we see that initially the mean momentum quickly drops to zero and the momentum variance rises as the quantum wave packet becomes delocalised. This is due to the nonlinear dependence of  $E_n(p)$  on the quantum number  $n$ . The decrease in momentum variance when  $s$  is a multiple of 150 indicates a revival of the initial wave packet. As in the classical dynamics of a distribution of points we find that as  $\epsilon$  increases from 0.0 to 0.2 the growth in the quantum momentum variance is suppressed and the mean becomes fixed about its initial value, indicating that the state is being localised.

In Fig. 13 we have represented the probability distribution of the state  $|\psi\rangle$  in the  $\epsilon = 0.2$  basis of quasi-stationary states. The length of each phasor  $\chi_m$  equals the overlap probability  $|\langle e_n, 0 | \psi \rangle|^2$  and its angle equals the eigenphase  $-2\pi e_n(0)/\hbar$ . We see that support on the quasi-stationary states has decreased to two states with almost identical quasi-energies. These states have opposite parity and we denote the even and odd states by  $|e_+, 0\rangle$  and  $|e_-, 0\rangle$  respectively.

In Fig. 14 we have expanded  $|e_-, 0\rangle$  in terms of the unperturbed stationary states  $|E_n, 0\rangle$ . We find that it is a superposition of a dominant state  $|E_{11}, 0\rangle$  and two other states  $|E_9, 0\rangle$  and  $|E_{13}, 0\rangle$  satisfying the near-resonant conditions

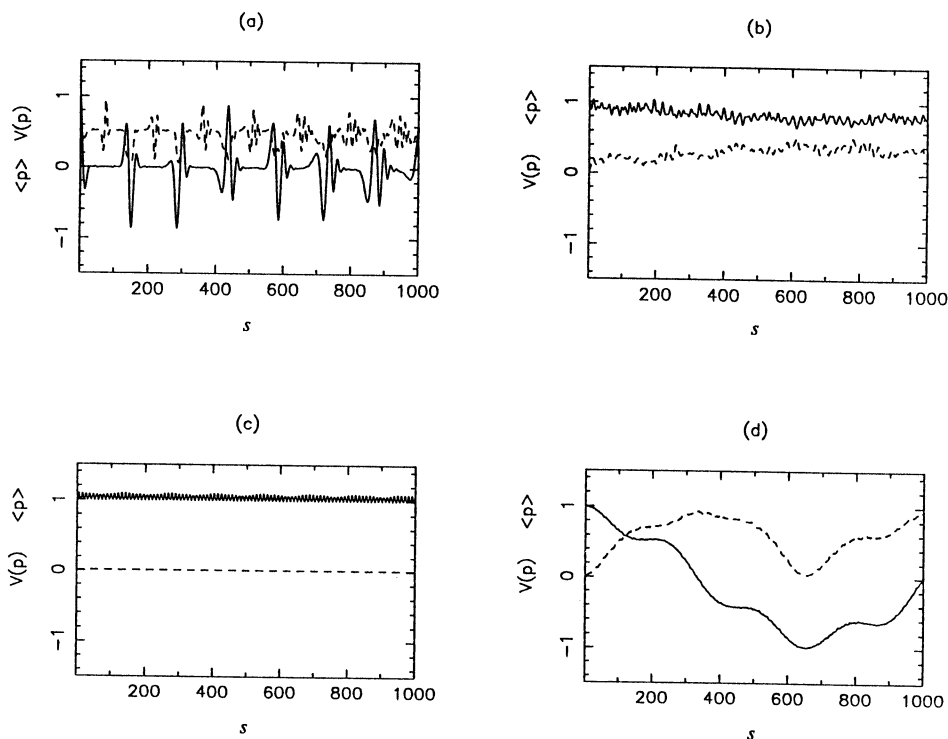


**Fig. 12.** Plot of quantum momentum statistics versus strobe number  $s$ : (a)  $\epsilon = 0.0$ , (b)  $\epsilon = 0.1$ , (c)  $\epsilon = 0.2$  and (d)  $\epsilon = 0.3$ . Solid line,  $\langle \hat{p} \rangle$ ; dashed line,  $V(\hat{p})$ .

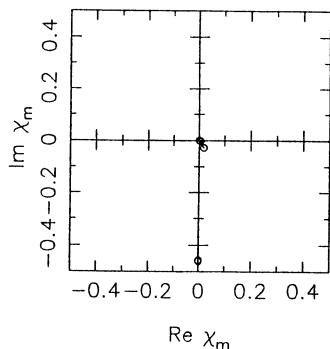


**Fig. 13.** Quasi-stationary state distribution of a minimum-uncertainty state, with  $\epsilon = 0.2$ .

$$E_{11}(0) - E_9(0) = 0.103 \approx 2k, \quad (73)$$

$$E_{11}(0) - E_{13}(0) = -0.101 \approx -2k. \quad (74)$$

We have plotted the  $Q$  function for  $|w_- \rangle$  in Fig. 15. The second-order resonance has caused the resonant quasi-stationary states to become strongly peaked about the classical stable fixed points, such that the initial minimum-uncertainty state

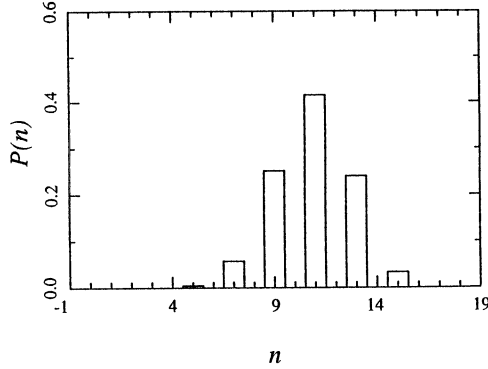


**Fig. 14.** Expansion of perturbed eigenstate  $|e_-, 0\rangle$  for  $\epsilon = 0.2$  in terms of the stationary standing-wave eigenstates  $|E_n, p\rangle$ :  $P(n) = |\langle E_n, 0 | e_-, 0 \rangle|^2$ .

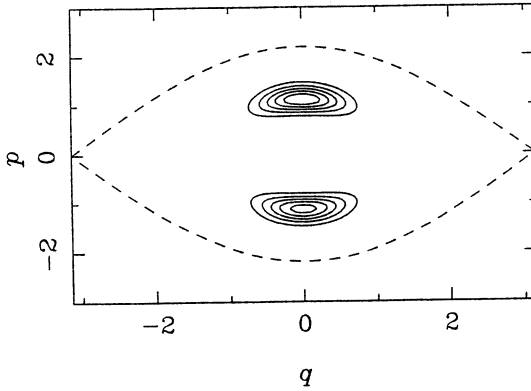


**Fig. 15.** The  $Q$  function of the Floquet operator eigenstate  $|e_-, 0\rangle$ .

is approximated by a sum of two states with opposite parity. These two states have almost identical quasi-frequencies so the minimum-uncertainty state changes slowly.

Since the minimum-uncertainty state is the sum of two quasi-stationary states with opposite parity we would expect to find coherent tunnelling between the region  $(q, p) \approx (0.0, 1.2)$  and its reflected partner  $(q, p) \approx (0.0, -1.2)$ . This is precisely what we see in Fig. 12d when  $\epsilon = 0.3$ .

#### 4.2 Standing Wave with Modulated Phase

Graham *et al.* (1992) proposed that a beam of ytterbium atoms prepared in their ground state be scattered from an optical standing wave. The position of the nodes of the standing wave would be made to oscillate at a frequency  $\omega$  and with an amplitude  $\lambda/2k$ , where  $k$  is the wavenumber of the standing wave

defined earlier. Classical mechanics describes this system by the following optical potential in dimensionless variables:

$$V(q, t) = -\kappa \cos(q - \lambda \sin t) . \quad (75)$$

The standing-wave phase changes sinusoidally, which may be accomplished by retro-reflecting a laser beam from an oscillating mirror. For large  $\lambda$  the gradient force varies too fast to affect the motion of the atom. In this case Hamilton's equations will correspond to free motion of the atom. This can be made more formal through the following change of variables:  $P = p/\sqrt{\lambda}$ ,  $Q = q$ ,  $\tau = \sqrt{\lambda}t$ . The Hamiltonian for these variables is

$$H = \frac{P^2}{2} - \epsilon \cos[Q - \lambda \sin \Omega \tau] , \quad (76)$$

where  $\Omega = 1/\sqrt{\lambda}$  and  $\epsilon = \kappa/\lambda$ . For  $\lambda$  much larger than  $\kappa$  this Hamiltonian describes a perturbation of the free motion with  $\epsilon$  playing the role of a perturbation parameter. For  $\epsilon = 0$ ,  $P$  and  $Q$  are the action-angle variables. The unperturbed frequency of motion is just  $\omega_{c1}(P) = P$ . To find the position of the first-order resonances we expand the perturbation as a Fourier series in  $\Omega\tau$ :

$$\cos[Q - \lambda \sin \Omega \tau] = \sum_{m=-\infty}^{\infty} J_m(\lambda) \cos(Q - m\Omega\tau) . \quad (77)$$

We see that first-order resonances will occur when  $P = m\Omega$ . Formally there are an infinite number of resonances but the Bessel function  $J_m(\lambda)$  decays exponentially with  $m$  for  $|m| > |\lambda|$  so that the resonances will be confined to the region  $|p| < |\lambda|$ .

The width in action of the resonance  $\Delta P$  can be read from (77) and is found to be

$$\Delta P = 2\sqrt{\epsilon|J_m(\lambda)|} . \quad (78)$$

The distance in action between resonances is just  $\delta P = \Omega$ . When  $\delta P \approx \Delta P$  the resonances interact with each other and can no longer be treated as isolated. If the resonances are sufficiently close all intervening invariant curves will have been destroyed and replaced by globally chaotic motion. The transition to global chaos can be estimated by the following resonance overlap criteria (Lichtenberg and Lieberman 1992):

$$\frac{2\Delta P}{\delta P} \approx \frac{2}{3} . \quad (79)$$

To estimate the average width of the resonances we approximate the Bessel function by its rms value  $J_m(\lambda) \approx 1/\sqrt{\pi\lambda}$  (Abramowitz and Stegun 1965) and find that stochastic trajectories fill the region  $|p| < |\lambda|$  when

$$\kappa > \kappa_c , \quad (80)$$

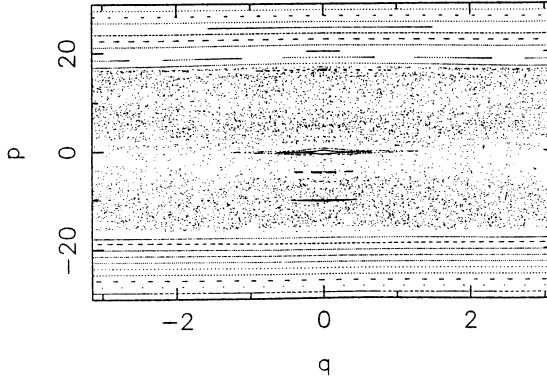


**Fig. 16.** Stroboscopic phase portrait of a classical ground state atom in a standing wave with a modulated node position, with  $\kappa = 1.2$ ,  $\lambda = 13.56$ .

where the critical parameter for global chaos is  $\kappa_c = (\sqrt{\pi\lambda}/36)$ . Graham *et al.* (1992) suggested a mirror driving frequency of  $\omega/2\pi = 125$  kHz. For these parameters  $\kappa = 1.2$ . In Fig. 16 we show the classical phase portrait for  $\lambda = 13.56$ , for which  $\kappa_c = 0.18$ . Notice that apart from a few stable elliptic fixed points with small widths in momentum the region  $p < 15$  is dominated by chaotic trajectories.

If a classical distribution is initially localised in the chaotic phase space, in time it will diffuse over the chaotic region  $-\lambda < p < \lambda$  and the momentum variance will be bounded by

$$V(p) = \lambda^2/3. \tag{81}$$

The study of classical diffusion is most conveniently done by replacing the Hamiltonian (76) by an approximation to the Floquet mapping.

We can formally integrate over one period  $T = 2\pi/\Omega$  of the driving to give the stroboscopic change in  $P$  and  $Q$ . We can find the change in  $P$  to first-order in  $\epsilon$  by integrating over the unperturbed value of  $Q$ . The first-order change in  $Q$  is then found by integrating over the first order perturbed value of  $P$ . The result is the following perturbed mapping:

$$\bar{P} = P + \epsilon f(\bar{P}, Q), \tag{82}$$

$$\bar{Q} = Q + T\bar{P} + \epsilon g(\bar{P}, Q), \tag{83}$$

where  $f$  and  $g$  are the following mixed functions of the new momentum and the old position:

$$f(\bar{P}, Q) = \sum_{m=-\infty}^{\infty} \frac{J_m(\lambda)}{\bar{P} - m\Omega} [\cos(Q + \bar{P}T) - \cos Q], \tag{84}$$

$$g(\bar{P}, Q) = \sum_{m=-\infty}^{\infty} \frac{J_m(\lambda)}{(\bar{P} - m\Omega)^2} [\sin(Q + \bar{P}T) - \sin Q] - T \sum_{m=-\infty}^{\infty} \frac{J_m(\lambda)}{\bar{P} - m\Omega} \cos(Q + \bar{P}T). \quad (85)$$

Equation (82) is an implicit equation for  $\bar{P}$ . Since we want to estimate the momentum diffusion it is more useful to deal with an explicit mapping. It can be made explicit by linearising  $f$  and  $g$  about a resonant trajectory  $\bar{P} = m\Omega$ . In terms of the old variables the approximate Floquet map is given by

$$\bar{p} = p - 2\pi \frac{\kappa}{\sqrt{\pi\lambda}} \sin q, \quad (86)$$

$$\bar{q} = q + 2\pi\bar{p}. \quad (87)$$

Once again we have replaced the Bessel function by its rms value. This approximation is the well known Chirikov–Taylor or standard mapping (Lichtenberg and Lieberman 1992).

In regions of phase space where the motion is globally stochastic it is possible to describe the evolution of the action using a diffusion process. The random-phase approximation assumes that after one period the atomic position is completely decorrelated from its initial value. This gives a diffusion constant of  $D_p = 2\pi\kappa^2/\lambda$  (see p. 329 of Lichtenberg and Lieberman 1992). For the values  $\kappa = 1.2$  and  $\lambda = 13.56$ , the random-phase approximation gives  $D_p \approx 0.67$ , which is in reasonable agreement with the numerically determined diffusion of the atomic momentum.

#### 4.2.1 Quantum

We will now turn to the question of how the atomic centre-of-mass dynamics is modified by quantum mechanics. For the experimental parameters proposed by Graham *et al.* (1992) the dimensionless Planck constant has the value  $\hbar = 0.24$ . Fig. 17 shows the quantum and classical momentum variance of a ground-state atom in the oscillating standing wave. Notice that the quantum mechanical momentum only diffuses for a short time, after which the momentum variance remains roughly constant. The quantum mechanical suppression of classical diffusion is called *dynamic localisation*.

Graham *et al.* (1992) approximated the dynamics by quantising the standard map approximation to the classical mapping, equations (86) and (87),

$$\hat{F} \approx \exp\left(\frac{-i\pi\hat{p}^2}{\hbar}\right) \exp\left(-2\pi i \frac{\kappa}{\sqrt{\pi\lambda}} \cos \hat{q}\right). \quad (88)$$

Let  $|e_n, p\rangle$  be an eigenstate of  $\hat{F}$ ; then using the transformation

$$u_m(p) = \frac{1 + \exp(-i2\pi e_n(p) + i\pi p^2/\hbar)}{2} \langle p + m\hbar | e_n, p \rangle, \quad (89)$$

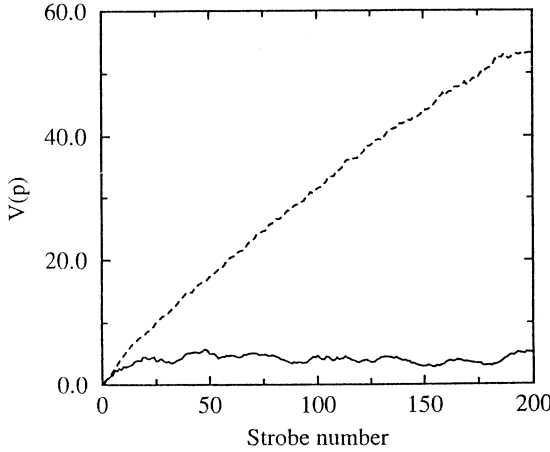


**Fig. 17.** Classical and quantum mechanical momentum variance as a function of strobe number for the oscillating standing wave with  $\kappa = 1.2$  and  $\lambda = 13.56$ : solid line, quantum scattering  $\hbar = 0.24$ ; dashed line, classical scattering.

the Floquet eigenvalue problem (62) now takes the form

$$T_m(p)u_m(p) - \sum_{r \neq 0} W_r u_{m+r}(p) = W_0 u_m(p), \tag{90}$$

where

$$T_m(p) = \tan \left( \frac{2\pi e_\mu(p) - \pi(p + m\hbar)^2/2\hbar}{2} \right), \tag{91}$$

$$W_r = \frac{1}{2\pi} \int_0^{2\pi} dq \tan \left( \frac{\sqrt{\pi}\kappa}{\lambda} \cos q \right) \exp(irq). \tag{92}$$

Equation (90) looks like a tight-binding problem for an electron in a one-dimensional crystal in which  $m$  labels the lattice positions,  $T_m(p)$  are the site free energies and  $W_r$  is the amplitude per unit time to make a transition from site  $m$  to site  $m + r$ . Grempel *et al.* (1984) argued that if  $\{T_m(p)\}$  is a quasi-random sequence of numbers then the spectral properties of (90) can be approximated by replacing it with a random sequence of numbers. Such a model was first studied by Anderson (1958, 1978). For a discussion of the conditions that  $\{T_m(p)\}$  must satisfy in order to be a quasi-random sequence, the reader is referred to the papers by Fishman *et al.* (1982) and Grempel *et al.* (1984). From now on we will assume that the appropriate conditions are satisfied and just mention the relevant conclusions of the Anderson model.

It is known (Fishman *et al.* 1982; Grempel *et al.* 1984; Shepelyansky 1986; Chirikov *et al.* 1989) that all eigenstates are localised around some lattice site and decay exponentially away from that site with a characteristic length  $l$  given by

$$l = \frac{D_p}{2\hbar^2}. \quad (93)$$

This fundamental result relates the rate of classical diffusion  $D_p$  to the quantum mechanical localisation length. A state localised at  $n = 0$  will develop into an exponentially localised distribution with a localisation length given by  $l_D = 2l$ . This predicts that the initial quantum state in Fig. 17 will have a steady-state variance of  $V(p) \approx (\hbar l_D)^2/2$ . For  $\kappa = 1.2$ ,  $\lambda = 13.56$ , and  $\hbar = 0.24$  the random-phase approximation for the classical diffusion constant gives steady-state momentum variance  $V(p) \approx 3.9$ , which is in good agreement with the numerical results in Fig. 17.

A group led by M. G. Raizen at the University of Texas at Austin have performed a similar experiment using laser-cooled sodium atoms (Moore *et al.* 1994; Robinson *et al.* 1995). They observed that for certain values of the driving amplitude  $\lambda$  the measured momentum variance was significantly less than the classical prediction. Measurements of the momentum distribution confirmed that the localisation was exponential. These experiments confirmed that in some cases quantum mechanics suppresses classical chaos.

### 4.3 Modulated Evanescent Wave

If the intensity of the evanescent wave is modified we add to the unperturbed Hamiltonian Eq.(50) the time-dependent potential

$$V(q, t) = \epsilon \kappa \cos(\omega_D t) e^{-q}, \quad (94)$$

where  $\omega_D$  is the modulation, or driving, frequency and typically  $\epsilon < 1$ . In Fig. 18a we plot the stroboscopic phase portrait (momentum versus position) for the unperturbed nonlinear oscillator for the case  $\lambda = 1$ ,  $\kappa = 1000$ . The nonlinear frequency decreases from the elliptic fixed point at  $q_0 = \ln(\kappa/\lambda)$  to a minimum at  $H_0 = \kappa$ , at which energy the atoms hit the surface.

If the perturbation is now turned on ( $\epsilon \neq 0$ ) rational curves are destroyed and replaced by an alternating sequence of elliptic and hyperbolic unstable points. To see this structure emerging, we view the phase-space orbits at fixed periods of the driving frequency. For example if  $(\omega(H_0)/\omega_D) = \frac{1}{2}$  we can expect to see a period-2 elliptic fixed point surrounded by a period-2 island structure. If we use the approximate expression for the nonlinear frequency  $\omega(H_0) = 2\pi/T_{cl}(H_0)$  for an infinite potential where  $T_{cl}(H_0)$  is given by (47), we find, for example, that for  $\lambda = 1$ ,  $\kappa = 1000$ ,  $\omega_D = 1$ , there is a period-2 fixed point near  $q = 19.7$ ,  $p = 0$ . In Fig. 18b we show a typical stroboscopic phase portrait for these parameters, with  $\epsilon = 0.3$ . A period-2 fixed point is found as expected near  $q = 20$ , in addition to many higher resonances and regions of chaotic motion.

To experimentally observe a stroboscopic phase portrait one might let atoms bounce vertically from the modulated evanescent wave and make stroboscopic measurements. It is not clear just what measurements could be used in this case.

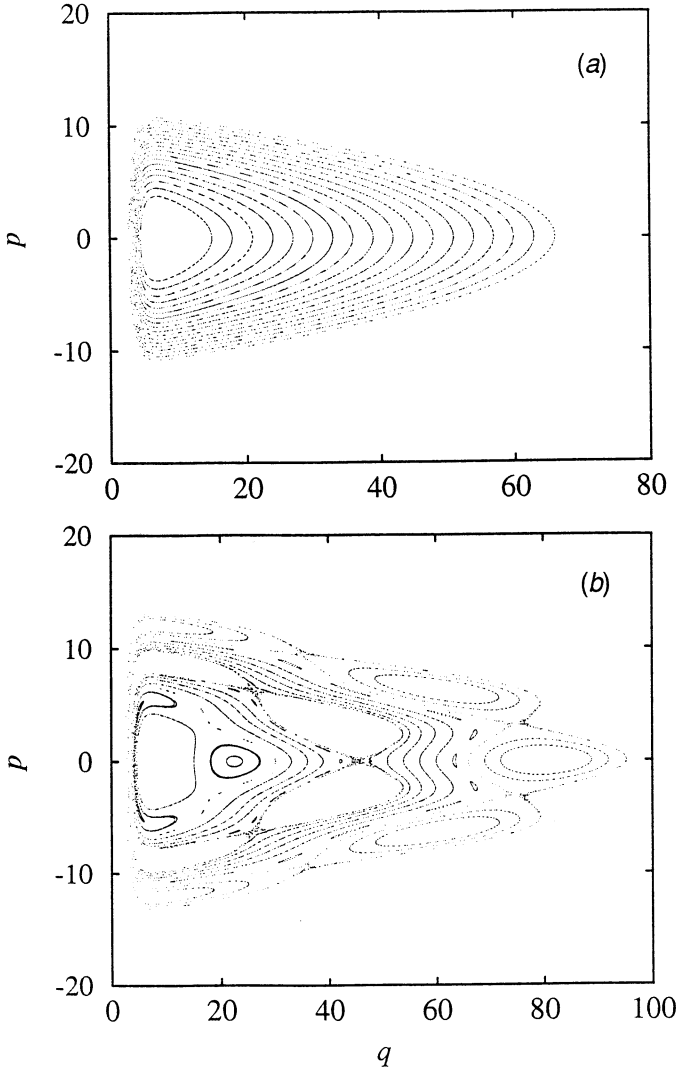


**Fig. 18.** Classical stroboscopic phase portraits for (a)  $\epsilon = 0.0$  and (b)  $\epsilon = 0.3$ .

Alternatively, if the atoms are given a velocity component parallel to the reflecting surface, a stroboscopic portrait may be constructed by making measurements only at fixed distances along the reflecting surface. A measurement of the momentum is more difficult, but could be done by probing the Doppler shift of the atoms with a sequence of laser fields at the appropriate spatial locations.

To estimate the values of the parameters we use the approximate classical expression for the period (47), which is valid provided  $q_0 \gg 1$ . A period- $n$  resonance then corresponds to an initial energy of

$$H_0 = \frac{1}{2} \left( \frac{n\pi\lambda}{\omega_D} \right)^2. \tag{95}$$

We take  $\alpha = 10^7 \text{m}^{-1}$  in (49). Consider the case of caesium atoms normally incident on an evanescent wave. In the experiment of Aminoff *et al.* (1993) reflections were seen for atoms dropped from an initial height of 3 mm. This fixes a minimum value for the potential at the surface of  $V_0 = 6.5 \times 10^{-27}$  J, so we take  $V_0 = 10^{-26}$  J. With this value, the parameters of the problem are given as  $T = 8 \times 10^{-5}$  s for the timescale factor,  $\lambda = 0.016$  for the scaled gravitational acceleration  $\kappa = 740$ . If an argon beam is used, the values of the parameters are  $T = 2.7 \times 10^{-4}$ ,  $\lambda = 0.18$  and  $\kappa = 28000 \cdot 0$ .

For a period-2 resonance with caesium, with  $\omega_D = 0.01$  (a frequency  $\approx 800$  Hz), we find that an initial height of 0.3 mm is required. For a period-2 resonance with argon, with  $\omega_D = 0.01$  (a frequency  $\approx 230$  Hz), an initial height of 3.6 mm is required. The value for caesium may be just within reach of current experiments. For a period-8 resonance with caesium and with  $\omega_D = 0.01$  an initial height of 5 mm is required. This height and modulation frequency should be within reach of current experiments.

## 5. Effect of Spontaneous Emission and Noise

In this section we give a brief presentation of the effect of spontaneous emission and noise on the nonlinear quantum dynamics of atoms. Simulations using a stochastic Schrödinger equation have been developed in some detail by Dum, Zoller and Ritsch (Dum *et al.* 1992*a*, 1992*b*) and Mølmer, Castin and Dalibard (Dalibard *et al.* 1992; Mølmer *et al.* 1993) and used to study dissipative nonlinear dynamics (Dyrting and Milburn 1995*a*). The quantum mechanical atom can be described by its internal state  $\sigma$ , which may take on values  $a$  or  $b$ , and a centre-of-mass state  $|\psi\rangle$ . The internal state changes according to the two jump processes  $N_1$  and  $N_2$ , which have the following actions:

$$a \xrightarrow{N_1} b, \quad (96)$$

$$b \xrightarrow{N_1} a, \quad (97)$$

$$b \xrightarrow{N_2} a. \quad (98)$$

These two jump processes proceed at the rates

$$E[dN_1] = \eta \langle \psi | f(\hat{q}/2, t)^2 | \psi \rangle dt, \quad (99)$$

$$E[dN_2] = \Gamma dt. \quad (100)$$

Here  $E[\ ]$  denotes an ensemble average. The centre-of-mass state evolves according to the un-normalised stochastic Schrödinger equation

$$\begin{aligned} d|\psi\rangle = & -\frac{i}{\hbar} dt \hat{K}_\sigma |\psi\rangle + dN_1 \left( \frac{f(\hat{q}/2, t)}{\sqrt{\langle f(\hat{q}/2, t)^2 \rangle}} - 1 \right) |\psi\rangle \\ & + dN_2 \left( \frac{\exp(i\bar{p}\hat{q}/\hbar)}{\sqrt{\langle \psi | \psi \rangle}} - 1 \right) |\psi\rangle, \end{aligned} \quad (101)$$

where  $\langle f(\hat{q}/2, t)^2 \rangle = \langle \psi | f(\hat{q}/2, t)^2 | \psi \rangle$ . This equation does not preserve the normalisation of the state  $|\psi\rangle$ . This will be important when we come to generate the times for the jump  $N_1$ . The jump terms determine the state after a jump  $|\psi_{\text{after}}\rangle$  in terms of the state before  $|\psi_{\text{before}}\rangle$  as follows:

$$N_1 : |\psi_{\text{after}}\rangle = \frac{f(\hat{q}/2, t) |\psi_{\text{before}}\rangle}{\sqrt{\langle \psi_{\text{before}} | f(\hat{q}/2, t)^2 | \psi_{\text{before}} \rangle}}, \quad (102)$$

$$N_2 : |\psi_{\text{after}}\rangle = \frac{\exp(i\bar{p}\hat{q}/\hbar) |\psi_{\text{before}}\rangle}{\sqrt{\langle \psi_{\text{before}} | \psi_{\text{before}} \rangle}}, \quad (103)$$

where  $\bar{p}$  is the random kick in momentum due to spontaneous recoil which satisfies

$$\text{Prob}(\bar{p}, \bar{p} + d\bar{p}) = \phi(\bar{p}) d\bar{p}. \quad (104)$$

The operator  $\hat{K}_\sigma$  is non-Hermitian and depends on the internal state  $\sigma$  as follows:

$$\hat{K}_\sigma = \begin{cases} \hat{p}^2/2 + V(\hat{q}, t)/\nu^*, & \sigma = a \\ \hat{p}^2/2 - V(\hat{q}, t)/\nu, & \sigma = b. \end{cases} \quad (105)$$

Between jumps the state evolves in a complex potential and the imaginary part of the complex potential causes the normalisation of  $|\psi\rangle$  to decay. The effect of an  $N_1$  jump is to change the internal state and to change the centre-of-mass state. The cumulative distribution function for the stimulated jump  $N_1$  is given by

$$P_{\text{stim}}(t) = 1 - |\langle \psi(t) | \psi(t) \rangle|. \quad (106)$$

We generate a random number  $z_{\text{stim}}$  which has a uniform distribution on the interval and provided that no spontaneous emission has occurred in the meantime, we integrate the wave equation with generator  $\hat{K}_\sigma$  to the time  $t$  such that  $z_{\text{stim}} = 1 - |\langle \psi(t) | \psi(t) \rangle|$ . In this way we compute when an atom makes a stimulated transition.

When the atom makes a transition to state  $b$  it is easy to generate the random number  $t_{\text{spont}}$  equal to the time at which the atom spontaneously emits using the cumulative distribution function  $P_{\text{spont}}(t) = 1 - \exp(-\Gamma t)$ . The effect of spontaneous emission  $N_2$  is to change the momentum of the state by the amount  $\bar{p}$  given by

$$\bar{p} = \hbar (\cos \zeta \cos \theta + \sin \phi \sin \theta \sin \zeta) / 2, \quad (107)$$

where  $\zeta$  is the angle between the dipole moment and the  $x$ -axis. The angle  $\phi \in [0, 2\pi]$  is random with a uniform distribution and  $\theta$  is given by

$$\theta = \arccos \left[ 2 \cos \left( \frac{\arccos(2y - 1) + 4\pi}{3} \right) \right], \quad (108)$$

where  $y \in [0, 1]$  is a random number with a uniform distribution. In our numerical calculations we have chosen  $\zeta = \pi/2$ .

To recover the centre-of-mass density operator one takes the ensemble average of the conditioned operators

$$\hat{\rho} = \hat{\rho}_a + \hat{\rho}_b = E \left[ \frac{|\psi\rangle\langle\psi|}{\langle\psi|\psi\rangle} \right]. \quad (109)$$

In our simulations we evolve a state  $|\psi\rangle$  forward for a time  $\delta t$  using the first-order split operator method (Feit and Fleck 1982). Then we calculate the norm of  $|\psi(t + \delta t)\rangle$  to see whether a stimulated jump has occurred and whether we reach the spontaneous emission time  $t_{\text{spont}}$ . If a jump occurs we apply the appropriate transformation (5) in the momentum representation and then evolve the new state forward  $\delta t$  and so on until it has been evolved forward the desired time. The whole process is then repeated over 1000 trajectories.

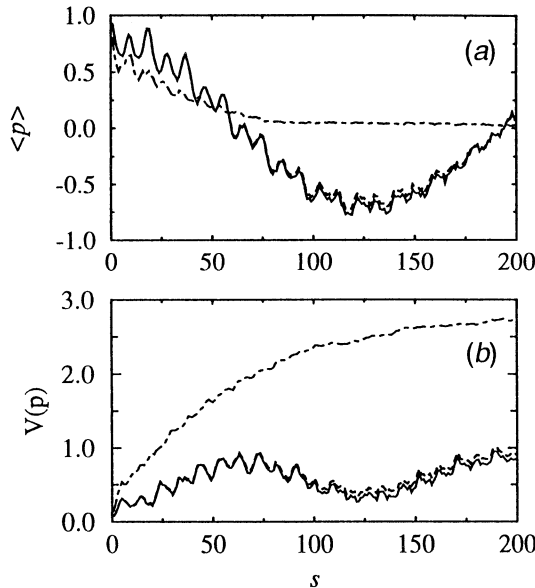


**Fig. 19.** Tunnelling between second-order resonances as reflected in (a) the momentum mean  $\langle p \rangle$  and (b) the variance  $V(p)$ . Solid line, coherent motion; dashed line, with spontaneous emission included and  $\Gamma = 1.525$ ,  $\eta = 6.1 \times 10^{-4}$ ; dot-dashed line,  $\eta = 0.02$ .

### 5.1 Modulated Intensity

To test whether spontaneous emission obscures coherent tunnelling we have done simulations using the atomic system of ytterbium mentioned earlier with  $k = 0.25$ , an initial wavepacket localised in phase space at  $(q_0, p_0) = (0.0, 1.0)$  and a momentum variance of  $V(p) = 0.04$ . In Fig. 19 we show quantum Monte Carlo simulations with and without spontaneous emission. We still see a definite sign of coherent tunnelling even when spontaneous emission is included.

For the initial state a semiclassical estimate for the coherence damping rate gives  $\Gamma_{\text{coh}} \approx 0.06\eta$ . The time taken to tunnel to the opposite second-order resonance is  $T \approx 125 \times 2\pi$ . This implies that the value  $\eta \approx 0.02$  is required for the critical damping of the tunnelling oscillations. Fig. 19 confirms that the coherent tunnelling is critically damped for this value of  $\eta$ .

### 5.2 Modulated Phase

Dynamic localisation is a coherent effect and noise due to spontaneous emission must be kept low. For the spontaneous decay rate of ytterbium of  $\gamma/2\pi = 183$  kHz, we have spontaneous and stimulated rates of  $\Gamma = 1.5$  and  $\eta = 4.5 \times 10^{-4}$  respectively. In Fig. 20 we have calculated the effect of spontaneous emission on the dynamic localisation. We see that for the parameters considered by Graham *et al.* (1992), dynamic localisation can still be clearly observed.

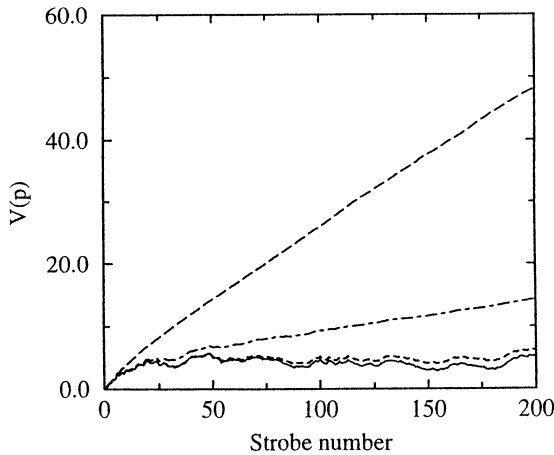


**Fig. 20.** Quantum momentum variance as a function of strobe number for a ytterbium atom in a standing wave with modulated phase;  $\kappa = 1.2$  and  $\lambda = 13.56$ . Solid line, scattering without spontaneous emission; dashed line, with spontaneous emission,  $\eta = 4.5 \times 10^{-4}$  and  $\Gamma = 1.525$ ; dot-dashed line,  $\eta = 4.5 \times 10^{-3}$ ; and long-dashed line,  $\eta = 4.5 \times 10^{-2}$ .

It is instructive to increase the stimulated rate  $\eta$  by factors of ten (see Table 1). In Fig. 20 we see that an increase in dissipation does destroy localisation. For strobe numbers greater than 50 the momentum does increase linearly but now quantum mechanics implies a decreased diffusion constant. This has also been

**Table 1. A comparison between dissipative diffusion rates measured using regression analysis and the value  $D_{\text{spont}}$**

The quantities  $D$  and  $r$  are the numerical diffusion rate and correlation coefficient respectively

$\epsilon$	$D$	$r$	$D_{\text{spont}}$
0.0	$-0.005 \pm 0.001$	-0.357	0.0
$4.5 \times 10^{-4}$	$0.002 \pm 0.001$	0.199	0.003
$4.5 \times 10^{-3}$	$0.050 \pm 0.001$	0.999	0.027
$4.5 \times 10^{-2}$	$0.228 \pm 0.001$	0.999	0.270

observed in models of the dissipatively kicked rotator (Dittrich and Graham 1990). Therefore, even for strongly dissipative systems in atomic optics, a signature of dynamic localisation would be a decrease in the scattered momentum diffusion rate. Dittrich and Graham have given a simple semi-quantitative treatment of dissipative diffusion in the quantum standard mapping, and we will now apply this estimate to our system. We assume that the standing-wave nodes oscillate so fast that the rate of incoherent absorption from the ground state is effectively averaged over a single wavelength to give  $\eta/2$ . Following Haake (1991), for weak dissipation and for times much greater than the break time  $l$  the new diffusion rate due to spontaneous emission is given by

$$D_{\text{spont}} = \pi \eta k^2 l^2. \quad (110)$$

We have measured the diffusion rates for the data given in Fig. 20 using linear regression analysis. In this calculation the points with strobe number less than 50 have been dropped. Although (110) gives a good estimate of the order of magnitude of the diffusion rates, it generally overestimates them.

### 5.3 Phase Noise

The experiments performed by Raizen's group (Moore *et al.* 1994; Robinson *et al.* 1995) to measure dynamic localisation were conducted under conditions where the effect of spontaneous emission is expected to be small. Another source of noise is the measurement process itself. Continuous measurement back-reaction tends to degrade quantum evolution and restore signatures of classical chaos. As yet there is no way of continuously measuring the momentum or position of an atom in a laser field, however, the effect of continuous measurement on the unconditioned evolution of the atom is equivalent to unitary evolution in the random potential (Dyrting and Milburn 1995*b*)

$$V(q, t) = \kappa \sin(q - \lambda \sin t + \phi), \quad (111)$$

where  $\phi$  is a continuous noise process added to the phase of the standing wave. When  $\phi$  is the Wiener process (Gardiner 1985)

$$\phi = \sqrt{\sigma} W, \quad (112)$$

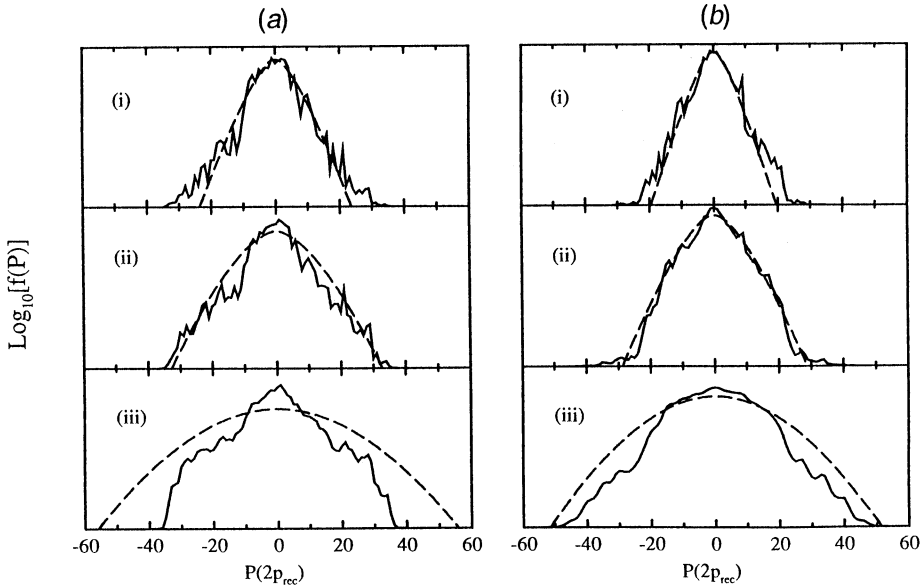


**Fig. 21.** Logarithm of the momentum distribution for sodium atoms in a modulated standing wave. Momentum is measured in units of  $\hbar$ . (a) Wiener noise,  $\lambda = 4.5$ : (i)  $\sigma = 0.0001$ ; (ii)  $\sigma = 0.001$ ; (iii)  $\sigma = 0.01$ . (b) Ornstein-Uhlenbeck noise,  $\lambda = 6.0$ :  $\eta = \sigma\kappa^2/k^2$ , (i)  $\eta = 0.0001$ ; (ii)  $\eta = 0.001$ ; (iii)  $\eta = 0.01$ .

where  $\phi$  is a continuous noise process added to the phase of the standing wave. When  $\phi$  is the Wiener process (Gardiner 1985)

$$\phi = \sqrt{\sigma}W, \tag{113}$$

the effect is the same as a continuous measurement of atomic momentum, and when  $\phi$  is the Ornstein-Uhlenbeck process

$$d\phi = -k\phi dt + \sqrt{\sigma} dW,$$

the effect is the same as a continuous measurement of the cosine of the atomic position. In the above equations  $k$  and  $\sigma$  are the damping and diffusion rates and  $W$  is the canonical Wiener process (Gardiner 1985). In Fig. 21 we show the effect of noise on the momentum distribution of sodium. The initial variance, the standing-wave amplitude and the Planck parameter are all equal to current experimental values:  $\sigma_p = (2.3\hbar)^2$ ,  $\kappa = 0.36$ ,  $\hbar = 0.16$ . The distribution has been calculated after 26 oscillation periods, which is approximately  $20 \mu\text{s}$  in the current experiments. We see that phase noise causes the momentum distribution to broaden. When the noise is weak there is good agreement with perturbation theory using the standard map approximation (88).

### 6. Summary

With current techniques in laser cooling and trapping it is possible to observe quantum mechanical motion of neutral atoms. Optical potentials are highly nonlinear, therefore atom optics can be used as a testing ground for quantum nonlinear dynamics. This view has been confirmed by recent experiments carried

out by Raizen's group (Moore *et al.* 1994; Robinson *et al.* 1995) which measured the dynamic localisation of atomic momentum. In this paper we have reviewed the basic concepts of nonlinear dynamics and applied them to the motion of atoms in time-dependent standing waves and to the atomic bouncing. We have compared classical and quantum nonlinear dynamics and discussed the feasibility of quantum effects being observed using current atom-manipulation techniques. Irreversible processes will tend to degrade the signatures of quantum nonlinear dynamics and restore classical behaviour. We have briefly discussed how this can happen in atom optics through spontaneous emission and phase noise.

## References and Bibliography

The following list contains work cited in the text, together with other material related to the topics discussed in this paper.

- Abramowitz, M., and Stegun, I. A. (1965). 'Handbook of Mathematical Functions' (USGPO: Washington, DC).
- Alber, G., Ritsch, H., and Zoller, P. (1986). *Phys. Rev. A* **34**, 1058.
- Aminoff, C. G., Steane, A. M., Bouyer, P., Desbiolles, P., Dalibard, J., and Cohen-Tannoudji, C. (1993). *Phys. Rev. Lett.* **71**, 3083.
- Anderson, P. W. (1958). *Phys. Rev.* **109**, 1492.
- Anderson, P. W. (1978). *Rev. Mod. Phys.* **50**, 191.
- Averbukh, I. Sh., and Perelman, N. F. (1989). *Phys. Lett.* **139**, 449.
- Balykin, V. I., Letokov, V. S., Ovchinnikov, Yu. B., and Sidrov, A. I. (1987). *Pis'ma Zh. Eksp. Teor. Fiz.* **45**, 282 [(1987). *JETP Lett.* **45**, 353].
- Berman, G. P., and Kolovsky, A. R. (1983a). *Phys. Lett. A* **95**, 15.
- Berman, G. P., and Kolovsky, A. R. (1983b). *Physica* **8D**, 117.
- Berman, G. P., and Zaslavsky, G. M. (1977). *Phys. Lett. A* **61**, 295.
- Berman, G. P., Zaslavsky, G. M., and Kolovsky, A. R. (1982). *Phys. Lett. A* **87**, 152.
- Berry, M. V., Balazs, N. L., Tabor, M., and Voros, A. (1979). *Ann. Phys. (New York)* **122**, 26.
- Blumel, R., Buchleitner, A., Graham, R., Sirko, L., Smilansky, U., and Walther, H. (1991). *Phys. Rev. A* **44**, 4521.
- Brune, M., Haroche, S., Lefevre, V., Raimond, J. M., and Zagury, N. (1990). *Phys. Rev. Lett.* **65**, 976.
- Carmichael, H. J. (1993). 'An Open Systems Approach to Quantum Optics' (Springer: Berlin).
- Casati, G., Chirikov, B. V., Izrailev, F. M., and Ford, J. (1979). In 'Stochastic Behaviour in Classical and Quantum Systems' (Eds G. Casati and J. Ford), p. 334 (Springer: Berlin).
- Chen, J., Story, J. G., Tollet, J. J., and Hulet, R. G. (1992). *Phys. Rev. Lett.* **69**, 1344.
- Chen, W.-Y., and Milburn, G. J. (1995). *Phys. Rev. A* **51**, 2328.
- Chirikov, B. V., and Shepelyansky, D. L. (1982). *Sov. Phys. Tech. Phys.* **27**, 156.
- Chirikov, B. V., Izrailev, F. M., and Shepelyansky, D. L. (1989). *Physica* **33D**, 77.
- Cohen-Tannoudji, C. (1992). In 'Fundamental Systems in Quantum Optics', Proc. Les Houches Summer School, Session LIII (Eds J. Dalibard *et al.*), p. 1 (Elsevier: Amsterdam).
- Cohen-Tannoudji, C., and Reynaud, S. (1979). *Phil. Trans. R. Soc. London A* **293**, 223.
- Cook, R. J., and Hill, R. K. (1982). *Opt. Commun.* **43**, 258.
- Courant, R., and Hilbert, D. (1989). 'Methods of Mathematical Physics' (Wiley: New York).
- Craig, W. (1983). *Commun. Math. Phys.* **88**, 113.
- Dalibard, J., and Cohen-Tannoudji, C. (1985). *J. Opt. Soc. Am. B* **2**, 1707.
- Dalibard, J., Castin, Y., and Mølmer, K. (1992). *Phys. Rev. Lett.* **68**, 580.
- Deutschmann, R., Ertmer, W., and Wallis, H. (1993). *Phys. Rev. A* **47**, 2169.
- Dinaberg, E. I., and Sinai, Ya. (1985). *Func. Anal. Appl.* **9**, 279.
- Dittrich, T., and Graham, R. (1990). *Ann. Phys. (New York)* **200**, 363.

- Dum, R., Parkins, A. S., Zoller, P., and Gardiner, C. W. (1992a). *Phys. Rev. A* **46**, 4382.
- Dum, R., Zoller, P., and Ritsch, H. (1992b). *Phys. Rev. A* **45**, 4879.
- Dwight, H. B. (1961). 'Tables of Integrals and Other Mathematical Data' (MacMillan: New York).
- Dyrting, S., and Milburn, G. J. (1993). *Phys. Rev. A* **47**, R2484.
- Dyrting, S., and Milburn, G. J. (1994). *Phys. Rev. A* **49**, 4180.
- Dyrting, S., and Milburn, G. J. (1995a). *Phys. Rev. A* **51**, 3136.
- Dyrting, S., and Milburn, G. J. (1995b). *Quant. Semiclassical Optics*, to be published.
- Dyrting, S., Milburn, G. J., and Holmes, C. A. (1993). *Phys. Rev. E* **48**, 969.
- Feit, M. D., and Fleck Jr, J. A. (1982). *J. Chem. Phys.* **78**, 412.
- Fishman, S., Grepel, D. R., and Prange, R. E. (1982). *Phys. Rev. Lett.* **49**, 509.
- Forest, E., and Berz, B. (1989). In 'Lie Methods in Optics II' (Ed. K. B. Wolf), p. 47 (Springer: Berlin).
- Gardiner, C. W. (1985). 'Handbook of Stochastic Methods' (Springer: Berlin).
- Gardiner, C. W., Parkins, A. S., and Zoller, P. (1992). *Phys. Rev. A* **46**, 4363.
- Goldstein, H. (1980). 'Classical Mechanics' (Addison-Wesley: Massachusetts).
- Graham, R., Schlautman, M., and Shepelyansky, D. L. (1991). *Phys. Rev. Lett.* **67**, 255.
- Graham, R., Schlautman, M., and Zoller, P. (1992). *Phys. Rev. A* **45**, R19.
- Grepel, D. R., Prange, R. E., and Fishman, S. (1984). *Phys. Rev. A* **29**, 1639.
- Grobe, R., and Haake, F. (1987). *Z. Phys. B* **68**, 503.
- Grossman, F., Jung, P., Dittrich, T. and Hänggi, P. (1991a). *Z. Phys. B* **84**, 315.
- Grossman, F., Jung, P., Dittrich, T. and Hänggi, P. (1991b). *Phys. Rev. Lett.* **67**, 516.
- Guckenheimer, J., and Holmes, P. (1983). 'Nonlinear Oscillations, Dynamical Systems and Bifurcations of Vector Fields' (Springer: New York).
- Haake, F. (1991). 'Quantum Signatures of Chaos' (Springer: Berlin).
- Hajnal, J. V., and Opat, G. I. (1989). *Opt. Commun.* **71**, 119.
- Hajnal, J. V., Baldwin, K. G. H., Fisk, P. T. H., Bachor, H.-A., and Opat, G. I. (1989). *Opt. Commun.* **73**, 331.
- Hawkes, A. G. (1971). *Biometrika* **58**, 83.
- Henkel, C., Steane, A. M., Kaiser, R., and Dalibard, J. (1995). *J. Physique II* **4**, 1877.
- Holland, J. S. (1992). In 'Schrodinger Operators: The Quantum Many-Body Problem' (Ed. E. Baslev), p. 100 (Springer: Berlin).
- Holland, M. J., Walls, D. F., and Zoller, P. (1991). *Phys. Rev. Lett.* **67**, 1716.
- Jessen, P. S., Gerz, C., Lett, P. D., Phillips, W. D., Rolston, S. L., Spreeuw, R. J. C., and Westbrook, C. I. (1992). *Phys. Rev. Lett.* **69**, 49.
- Kasevich, M. A., Weiss, D. S., and Chu, S. (1990). *Opt. Lett.* **15**, 607.
- Kazentsev, A. P., Surdutovich, G. I., and Yakovlev, V. P. (1980). *Sov. Phys. JETP Lett.* **31**, 509.
- Kazentsev, A. P., Surdutovich, G. I., Yakovlev, V. P., and Chudesnikov, D. O. (1985). *Opt. Commun.* **52**, 311.
- Kazentsev, A. P., Surdutovich, G. I., and Yakovlev, V. P. (1990). 'Mechanical Action of Light on Atoms' (World Scientific: Singapore).
- Kittel, C. (1962). 'Elementary Solid State Physics: A Short Course' (Wiley: New York).
- Kittel, C. (1976). 'Introduction to Solid State Physics' (Wiley: New York).
- Kosloff, R. (1988). *J. Phys. Chem.* **92**, 2087.
- Kreyszig, E. (1978). 'Introductory Functional Analysis' (Wiley: New York).
- Lichtenberg, A. J., and Lieberman, M. A. (1992). 'Regular and Chaotic Dynamics' (Springer: New York).
- Lin, W. A., and Ballentine, L. E. (1990). *Phys. Rev. Lett.* **65**, 2927.
- Lin, W. A., and Reichl, L. E. (1989). *Phys. Rev. A* **40**, 1055.
- Littlejohn, R. G. (1986). *Phys. Rep.* **138**, 194.
- Loudon, R. (1983). 'The Quantum Theory of Light' (Oxford Univ. Press).
- Louisell, W. H. (1973). 'Quantum Statistical Properties of Radiation' (Wiley: New York).
- Merzbacher, E. (1970). 'Quantum Mechanics' (Wiley: New York).
- Milburn, G. J. (1985). *Phys. Rev. A* **33**, 674.
- Mølmer, K., Castin, Y., and Dalibard, J. (1993). *J. Opt. Soc. Am. B* **10**, 524.
- Moore, F. L., Robinson, J. C., Bharucha, C., Williams, P. E., and Raizen, M. G. (1994). *Phys. Rev. Lett.* **73**, 2974.

- Nikitin, E. E., and Pitaevskii, L. P. (1994). *Phys. Rev. A* **49**, 695.
- Parker, J., and Stroud Jr, C. R. (1986). *Phys. Rev. Lett.* **56**, 716.
- Pool, R. (1992). *Science* **255**, 1513.
- Press, W. H., Teukolsky, S. A., Vetterling, W. T., and Flannery, B. R. (1992). 'Numerical Recipes in C' (Cambridge Univ. Press: New York).
- Rechester, A. B., and White, R. B. (1980). *Phys. Rev. Lett.* **44**, 1586.
- Rempe, W., Walther, H., and Klein, N. (1987). *Phys. Rev. Lett.* **58**, 353.
- Risken, H. (1984). 'The Fokker-Planck Equation' (Springer: Berlin).
- Robinson, J. C., Bharucha, C., Moore, F. L., Jahnke, R., Georgakis, G. A., Niu, Q., Raizen, M. G., and Sundaram, B. (1995). *Phys. Rev. Lett.* **74**, 3963.
- Ruth, R. D. (1983). *IEE Trans. Nucl. Science* **NS-30**, 2669.
- Sambe, H. (1973). *Phys. Rev. A* **7**, 2203.
- Sanders, B. C. (1989). *Phys. Rev. A* **40**, 2417.
- Sanders, B. C., and Milburn, G. J. (1989). *Z. Phys. B* **77**, 497.
- Seifert, W., Adams, C. S., Balykin, V. I., Heine, C., Ovichunikov, Yu., and Mlynek, J. (1994). *Phys. Rev. A* **49**, 3814.
- Shepelyansky, D. L. (1986). *Phys. Rev. Lett.* **56**, 677.
- Shepelyansky, D. L. (1987). *Physica* **28D**, 103.
- Slater, J. C. (1952). *Phys. Rev.* **87**, 807.
- Sleater, T., Pfau, T., Balykin, V., Carnal, O., and Mlynek, J. (1992). *Phys. Rev. Lett.* **68**, 1996.
- Stenlake, B. W., Littler, I. C. M., Bachor, H.-A., Baldwin, K. G. H., and Fisk, P. T. H. (1994). *Phys. Rev. A* **49**, R16.
- Tan, S. M., and Walls, D. F. (1995). *J. Physique II A* **4**, 1897.
- Tanguy, C., Reynaud, S., and Cohen-Tannoudji, C. (1984). *J. Phys. B* **17**, 4623.
- Wallis, H., Dalibard, J., and Cohen-Tannoudji, C. (1992). *Appl. Phys. B* **54**, 407.
- Walls, D. F., and Milburn, G. J. (1994). 'Quantum Optics' (Springer: Berlin).
- Wannier, G. (1937). *Phys. Rev.* **52**, 191.
- Wiseman, H. M. (1994). *Phys. Rev. A* **49**, 2133.
- Wiseman, H. M., and Milburn, G. J. (1993). *Phys. Rev. A* **47**, 1652.
- Yurke, B., and Stoler, D. (1986). *Phys. Rev. Lett.* **57**, 13.
- Zaslavsky, G. M. (1985). 'Stochasticity of Dynamical Systems' (Nauka: Moscow).